NASA Contractor Report 3448

Design, Development, and Field Testing of Infrared Heterodyne Radiometer (IHR) for Remote Profiling of Tropospheric and Stratospheric Species

R. Lange, M. Savage, and B. Peyton

NASA

NASA Contractor Report 3448

Design, Development, and Field Testing of Infrared Heterodyne Radiometer (IHR) for Remote Profiling of Tropospheric and Stratospheric Species

R. Lange, M. Savage, and B. Peyton
Eaton Corporation AIL Division
Melville, New York

NASA
National Aeronautics
and Space Administration

**Scientific and Technical
Information Branch**

1981

FOREWORD

Dimensional quantities are given in SI Units except for altitudes, which are given in feet to correspond to altimeter readings. To convert from feet to meters, multiply the value in feet by 0.3048.

TABLE OF CONTENTS

LIST OF ILLUSTRATIONS

1.0 INTRODUCTION

This report describes the results of a 2-1/2 year analytical, instrument development, feasibility demonstration, and flight-test program aimed at verifying that a new type of infrared radiometer can be employed to remotely monitor the concentration and vertical distribution of selected atmospheric species. The dual-channel Infrared Heterodyne Radiometer (IHR) was developed and flight tested under NASA's Advanced Applications Flight Experiment Office sponsorship. Based on the results of this program, it has been demonstrated that an IHR can be employed to remotely detect, monitor and track the concentration, vertical distribution, and spatial extent of natural and man-made atmospheric molecular constituents having a vibrational-rotational spectral line which overlaps the emission wavelength of the laser local oscillator source in the IHR. The IHR developed on this program utilizes CO_2 gas lasers which emit in discrete portions of the 9 to 11 μm wavelength region. Ongoing work with widely tunable semiconductor laser local oscillators offers the potential of covering a significantly larger portion of the infrared spectrum as well as most atmospheric species of interest with the next generation of IHR's.

A variety of atmospheric radiance and absorption measurements have been previously carried out using direct detection infrared radiometers.[1,2] However, recent development of wideband heterodyne detection techniques makes such measurements possible with nearly quantum-noise-limited sensitivity and ultrafine spectral resolution.[3-6] These features are of particular significance in remote sensing of atmospheric and pollutant gases where low-level spectral absorptions (emissions) exist in a background of other interfering gases. IHR spectral resolutions ranging from 10^{-4} to 6.7×10^{-2} cm^{-1} are possible, and provide the capability of examining individual atmospheric vibrational-rotational spectral (signature) lines. High spectral resolution heterodyne measurements of solar and astronomical radiances have been reported.[7-12] Several analyses illustrating the use of heterodyne detection for remote sensing of gas concentrations have been reported.[13-17] In particular, the potential of heterodyne measurements for inferring pollutant gas profiles from satellite measurements of atmospheric emissions[14] and from

measurements of reflected laser (hot source) absorption[15,16] have been discussed.

The IHR developed on this program employs two independent infrared channels. It utilizes a common collecting aperture, a common Dicke switch, and a common reference/calibration network. Each infrared channel of the IHR contains a wideband PV:HgCdTe photomixer, a CO_2 local oscillator (LO), and a wideband IF preamplifier.

The Dicke-switched IHR has been employed in both the solar absorption (SA) and the nadir radiance (NR) modes. In the SA mode, the IHR uses the sun as a back lighting thermal source for narrowband atmospheric absorption measurements of individual atmospheric spectral lines. In the NR mode, the IHR is pointed downward toward the earth's surface from an airborne platform and views the upwelling thermal radiance from the earth and the intervening atmosphere. Operation in the Limb Radiance and Solar Occultation modes, from the ground, have also been investigated.

The IHR employs an infrared channel which is selected to: (1) provide a reference radiance level of source irradiance which is in close spectral proximity to the atmospheric spectral line of interest and (2) be free of the degrading effects of other potentially interfering atmospheric gases. The other infrared channel of the IHR is chosen to overlap a single isolated vibrational-rotational spectral line of the selected atmospheric species. The pollutant IF bandwidth is split into a number of narrower channels which provide fine spectral resolution of the selected spectral line. This fine spectral data of the IHR is then used to generate vertical concentration profiles of the measured atmospheric gas using radiance inversion and line profile techniques.[13-17]

Ammonia (NH_3) and ozone (O_3) were chosen as the two atmospheric gases for the IHR feasibility demonstration. These gases are both important in studies of atmospheric processes and atmospheric pollution. In addition, tropospheric measurement data, particularly in the case of NH_3, are limited.

Atmospheric ammonia is involved in aerosol production[18] and may constitute a significant source or sink in NO_x chemistry.[19] Tropospheric ozone accounts for much of the pollution injury to vegetation[20] and excessive ozone levels are considered evidence of photochemical smog formation.[21]

Both ground-based and airborne IHR measurements have been carried out in order to verify the feasibility of obtaining remote profiles using this new radiometric instrument. The ground-based IHR measurements were carried

2

out at AIL, Melville, New York utilizing a solar tracking heliostat. The assembled IHR in the ground-based AIL solar observatory is shown in Figure 1-1. The IHR includes the optical package, four radiometric processors, the photomixer control and laser monitor panel, the reference/calibration black body and laser power supplies, the data management network, analog recorders, and digital recorders. The IHR was designed for both ground-based measurements and for operation in the NASA CV-990 test aircraft. Laboratory absorption measurements using an ammonia test cell and solar atmospheric absorption measurements of ammonia have been carried out. In March 1976, the first tropospheric ammonia profiling measurements were carried out using the newly developed IHR. Following the ground-based SA ammonia measurements, the IHR was converted to permit ground-based SA measurement of ozone by changing the gas fill of the CO_2 laser local oscillators.

The IHR was integrated into the NASA CV-990 "Gallileo II" test aircraft at NASA Ames in September 1976, and test flown on the Latitude Survey Mission between October and November 1976. These flights traveled from the North to the South Pole over the Pacific Ocean and stratospheric ozone measurements were carried out during the entire mission. From these measurements, profiles of the stratospheric ozone layer were determined at selected latitudes. A photograph of the IHR installed aboard the CV-990 test aircraft is shown in Figure 1-2.

Figure 1-1. Dual Laser, Multi-IF Channel, Dicke-Switched IHR
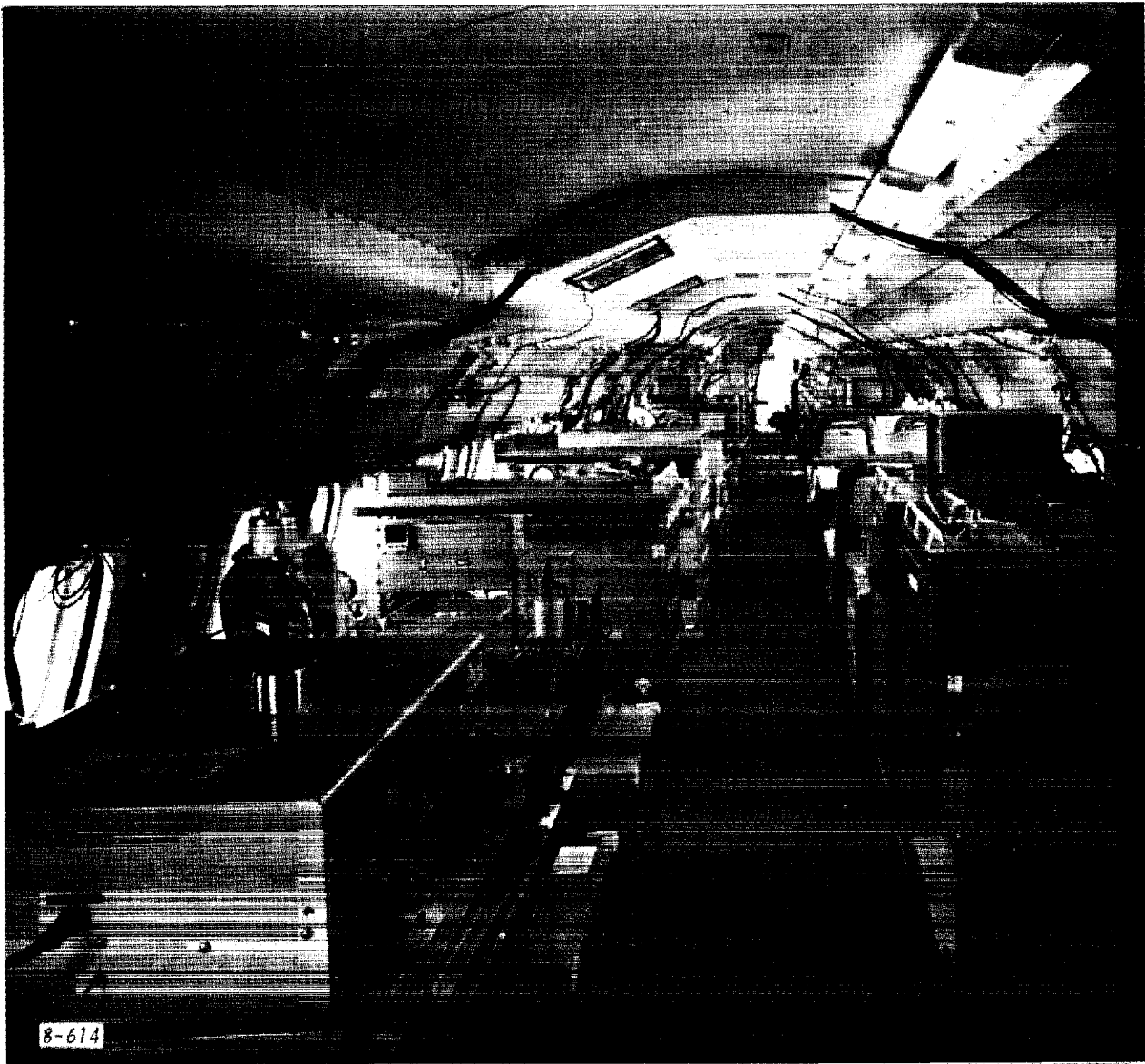
Figure 1-2. IHR Installation Aboard NASA CV-990

2.0 SELECTION OF LASER LO TRANSITIONS TO OVERLAP SPECTRAL LINES OF SELECTED ATMOSPHERIC SPECIES

One laser LO transition of the IHR is selected to spectrally overlap a selected vibrational-rotational spectral line of the atmospheric species of interest. Since the width of the selected spectral line changes with altitude, the required spectral proximity of the LO transition is fixed by: (1) the integrated width of the selected species spectral line over the intervening atmospheric path and (2) the IF bandwidth of the IHR.

The center frequency of the IHR spectral detection band is fixed by the laser LO frequency. The instantaneous bandwidth of the individual channels is fixed by IF filters, and the maximum useful IF frequency is fixed by the photomixer frequency response.

The signature spectral line of the selected atmospheric species used for remote atmospheric profiling is selected based on the following criteria:

- Strong absorption coefficient with suitable laser LO spectral proximity

- An isolated signature line of the selected atmospheric species

- Spectrally isolated for minimum interference from other atmospheric species

It should be noted that different species spectral lines may be selected for different IHR operating modes. For example, the large amount of stratospheric ozone dictates the use of a moderate strength (absorption) signature line for SA measurements while the relatively small amount of tropospheric ozone requires the use of a strong (absorption) signature line for NR measurements from an airborne platform.

Atmospheric gases with signature lines in the 9 to 11 μm region include NH_3, O_3, C_2H_4, HNO_3, H_2O, ClO, $CFCl_3$, and CF_2Cl_2. Whenever possible, $C^{13}O_2^{16}$ (or $C^{12}O_2^{18}$) minor isotopic laser LO's are preferred for remote IHR atmospheric measurements in order to eliminate the effects of interference and/or attenuation due to the normally abundant levels of atmospheric $C^{12}O_2^{16}$.

A comprehensive study of the overlap between CO_2 laser transitions and the suitable NH_3 and O_3 spectral signature lines was performed at NASA LaRC to determine optimum IHR operating wavelengths. Remote IHR measurements of upwelling atmospheric radiance (NR mode) and measurements of atmospheric absorption of solar radiance (SA mode) were investigated.[22] A line-by-line computer model[23] was used for all of the transmittance, absorption, and radiance calculations. This computer model considers both Lorentz and Voigt profile line shapes and includes temperature and pressure effects on the spectral line strengths and the spectral half widths. The effects of gaseous H_2O, CO_2, O_3, N_2O, SO_2 and NH_3 were also included.

Line parameter data for H_2O, CO_2, O_3, N_2O[24], and NH_3[25] were available in the existing literature, while the data for SO_2 came from an unpublished compilation by R. F. Calfee of NOAA. Ammonia absorption measurements[26] have been carried out with a $C^{13}O_2^{16}$ laser to verify the predicted signature line characteristics for ammonia, and tunable diode laser spectroscopy measurements have been carried out at LaRC to verify the predicted spectral positions of the ammonia and ozone spectral lines. A mid-latitude summer model atmosphere has been used to provide temperature and pressure profiles as well as water vapor and ozone altitude distributions. Estimates of the water vapor continuum absorption effects have also been included in the spectroscopic analysis.

The IHR measurements for atmospheric ammonia were carried out in the SA mode using the following CO_2 laser LO transitions:

SA Mode (NH_3)

Reference Channel - R(8) transition of $C^{13}O_2^{16}$ laser at 920.2195 cm^{-1}

Species Channel - R(18) transition of $C^{13}O_2^{16}$ laser at 927.3004 cm^{-1}

The calculated transmittance spectra between 920 cm^{-1} and 932 cm^{-1} for a 1-km atmospheric path length is shown in Figure 2-1. The first spectra is due to atmospheric ammonia alone and the second includes atmospheric ammonia as well as all the other major atmospheric constituents. The spectral overlap of the $C^{13}O_2^{16}$ laser LO transitions are also shown.
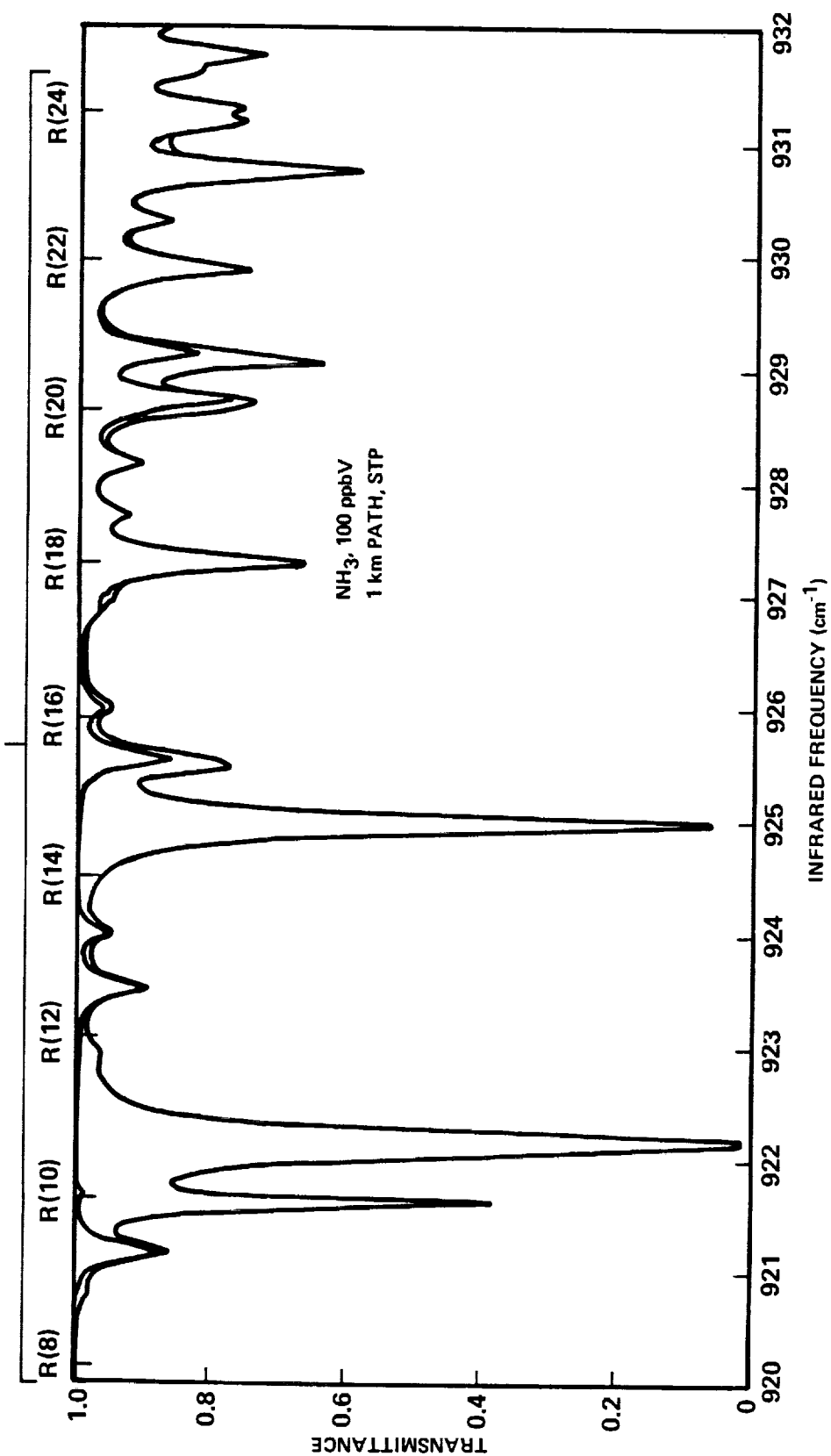
Figure 2-1. Calculated Atmospheric Transmittance of Ammonia and the Total Atmosphere as a Function of Frequency for a 1-km Path with $C^{13}O_2^{16}$ Laser Transition Overlaps

8

The IHR laser LO transitions initially chosen for the SA measurements of atmospheric ozone were:

SA Mode (O_3) (Initially Selected)

Reference Channel - R(10) transition of $C^{13}O_2^{16}$ at 1025.7783 cm^{-1}

Species Channel - P(18) transition of $C^{13}O_2^{16}$ at 1002.4776 cm^{-1}

The calculated transmittance spectra between 1000 cm^{-1} and 1030 cm^{-1} for a 1-km atmospheric path length is shown in Figure 2-2. The first spectra is due to atmospheric ozone alone, and the second includes atmospheric ozone as well as all the other major atmospheric constituents. The spectral overlap of the $C^{13}O_2^{16}$ laser LO transitions are also shown. However, it was found that the $C^{13}O_2^{16}$ isotopic mixture lasers available for the IHR measurements provided insufficient LO power for efficient heterodyne operation using these initially selected LO transitions. Therefore, the IHR profiling measurements of atmospheric ozone in the SA mode were carried out using a CO_2 laser with the normal isotopic gas mixture:

SA Mode (O_3)

Reference Channel - P(24) transition of $C^{12}O_2^{16}$ at 1043.1633 cm^{-1}

Species Channel - P(18) transition of $C^{12}O_2^{16}$ at 1048.8661 cm^{-1}

or   P(20) transition of $C^{12}O_2^{16}$ at 1046.8542

P(26) transition of $C^{12}O_2^{16}$ at 1041.2791

The CO_2 laser transitions selected for the IHR measurement of atmospheric ozone in the NR mode are:

NR Mode (O_3)

Reference Channel - P(24) transition of $C^{12}O_2^{16}$ at 1043.1633 cm^{-1}

Species Channel - P(14) transition of $C^{12}O_2^{16}$ at 1052.1959 cm^{-1}

9
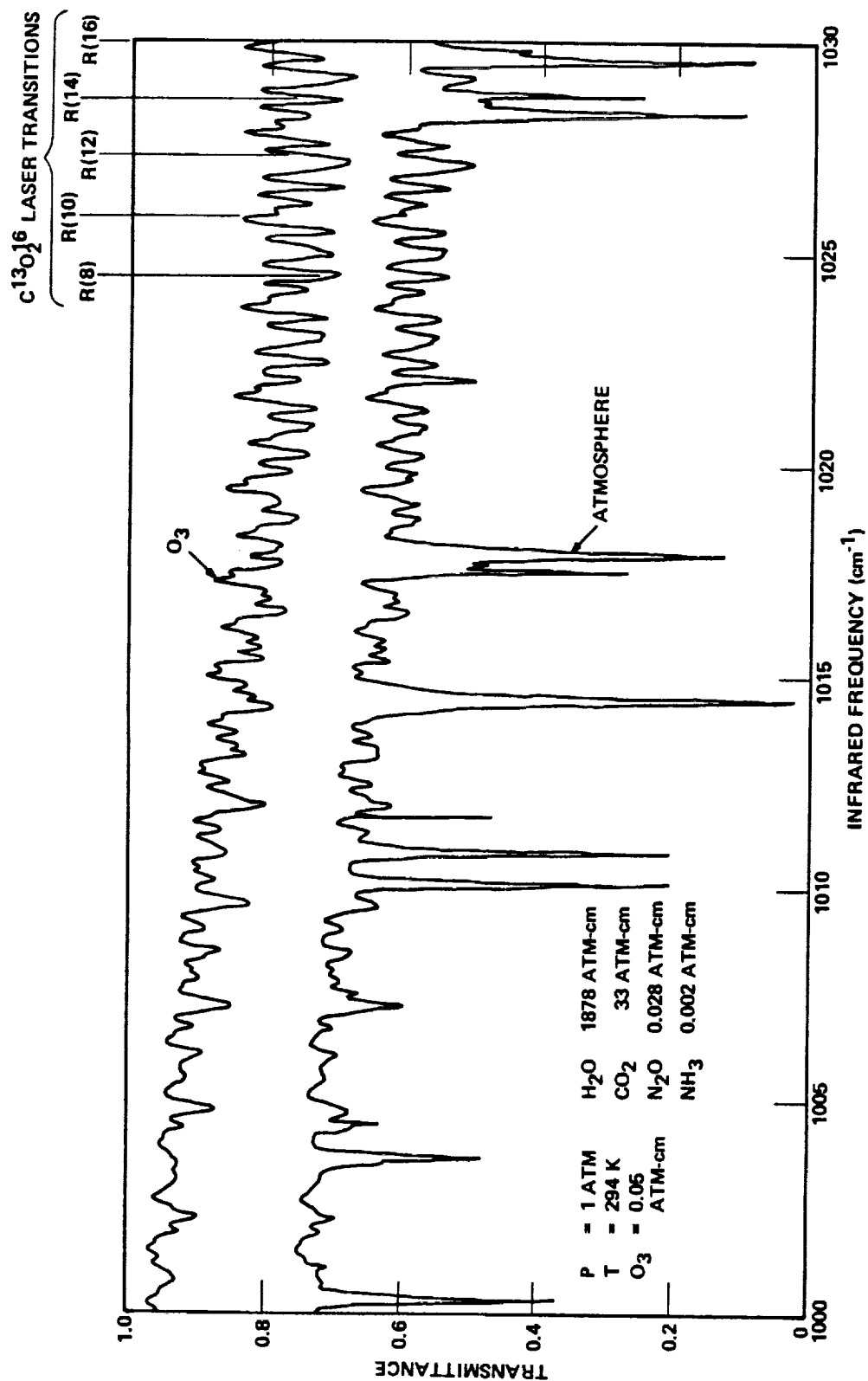
Figure 2-2. Calculated Atmospheric Transmittance of Ozone and the Total Atmosphere as a Function of Frequency for a 1-km Path with $C^{13}O_2^{16}$ Laser Transition Overlaps (1000 to 1030 cm^{-1})

10

The calculated transmittance spectra between 1040 cm^{-1} and 1055 cm^{-1} for a 1-km atmospheric path length is shown in Figure 2-3. The first spectra is due to atmospheric ozone alone, and the second includes atmospheric ozone as well as all the other major atmospheric constituents. The spectral overlap of the $C^{12}O_2^{16}$ laser LO transitions with discrete ozone spectral lines are also shown.
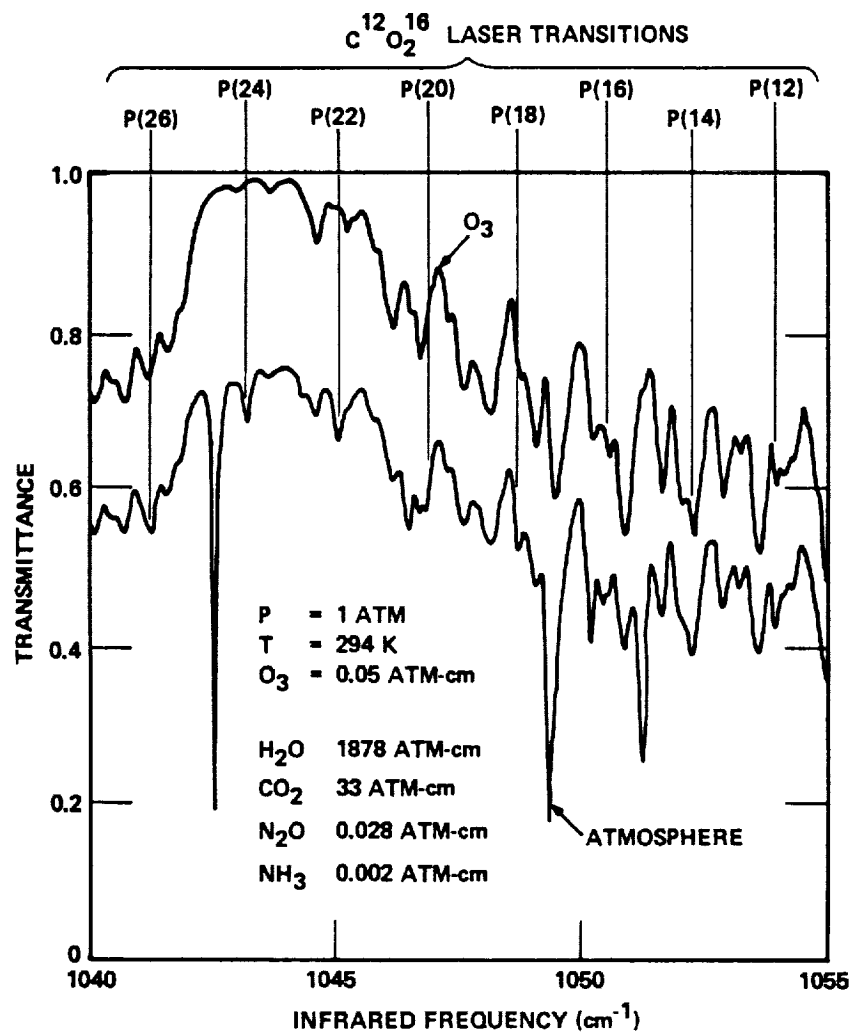
Figure 2-3. Calculated Atmospheric Transmittance of Ozone and the Total Atmosphere as a Function of Frequency for a 1-km Path with $C^{13}O_2^{16}$ Laser Transition Overlays (1040 to 1055 cm^{-1})

12

3.0 IHR SYSTEM CONCEPT

The IHR has been designed to operate in both the solar absorption (SA) and the nadir radiance (NR) measurement modes. Since the dual channel IHR is a new type of measurement instrument, special attention has been given to developing a versatile radiometer which can be used to demonstrate its ability to remotely detect, monitor, and track the concentration, vertical distribution, and spatial extent of natural and man-made atmospheric molecular species. The Dicke-switched dual photomixer IHR which has been developed offers the system advantages of:

- Incorporating a spectrally clear "reference" channel which is unaffected by the presence of the selected atmospheric species or other interfering gas absorptions. The reference channel reduces, or eliminates, the effects of water vapor continuum, slant path length variations, and temperature/emissivity changes in the backlighting infrared source.

- Minimizing the effects of the laser LO amplitude instabilities due to the use of a Dicke-switch.

- A 3-dB improvement in the overall system sensitivity because one of the two radiometer channels is always viewing the source irradiance.

- Using common collecting optics, Dicke-switch, optical train, and reference/calibrate black body sources. The use of common instrumentation in both infrared channels improves the accuracy of the overall measurement activities.

- The potential of simultaneously monitoring two atmospheric species for the case in which the back-lighting infrared source and the intervening atmospheric conditions are constant. This type of measurement is believed to be particularly important in studying the dynamics of atmospheric chemistry.

13

3.1 MEASUREMENT CONCEPT

The center frequencies of the two IHR infrared channels are fixed by the laser LO frequencies in the heterodyne detection mode. The instantaneous bandwidth of each of the IHR infrared channels is fixed by IF filters.

Following wideband IF amplification of the species channel photomixer output, the IF passband is power split into three separate IF channels in which the frequency and bandwidth are fixed by IF filters. This is equivalent to splitting the IHR infrared spectral passband and it can be conveniently carried out at IF frequencies because of the linear frequency translation properties of an infrared heterodyne receiver.[27] This spectral splitting of the infrared channel yields fine spectral signature data concerning the integrated atmospheric spectral line (Figure 3-1). It is this integrated spectral signature data which is used to derive information on the relative distribution of the species concentration with altitude.

The IF channel closest to line center in the species channel is affected by absorption and emission from all levels of the intervening atmosphere between the IHR and the source of irradiance. However, due to the collision broadening of the species linewidth with pressure (maximum near the earth's surface), the highest frequency IF channel of the IHR is affected primarily by the species concentrations near ground level. The IF channels of the IHR between these two extremes will, therefore, see more and more high altitude absorption or emission as the channel center frequency moves closer to the species absorption line center as the spectral linewidth narrows. Detection of stratospheric species will require a relatively narrowband ($\approx$1000 MHz) IHR when the selected species signature line and the laser LO transition are in close spectral proximity, while the measurement of tropospheric species will require wider instantaneous bandwidth IHR (B $\approx$ 2500 MHz). The IHR developed and tested on this program provided a species channel upper frequency limit of 2200 MHz.

As stated, the IHR development concepts were aimed at designing a flexible field-worthy instrument which could be used in either of two measurement modes: the SA and the NR. The SA measurement mode utilizes the sun as a hot black body source in order to measure the atmospheric transmission and therefore deduce the absorption of the selected atmospheric gas. This measurement mode can be used for several scenarios (that is, ground based, balloon borne and airborne). A solar tracking heliostat and a narrow field-of-view (FOV) radiometer are required so that the solar disc fills the FOV of the IHR. Ground-based measurements can provide a vertical profile of the species concentration in both the troposphere and the stratosphere. Aircraft platform SA measurements can provide profiles in the upper troposphere and stratosphere. Future satellite platform measurements

14
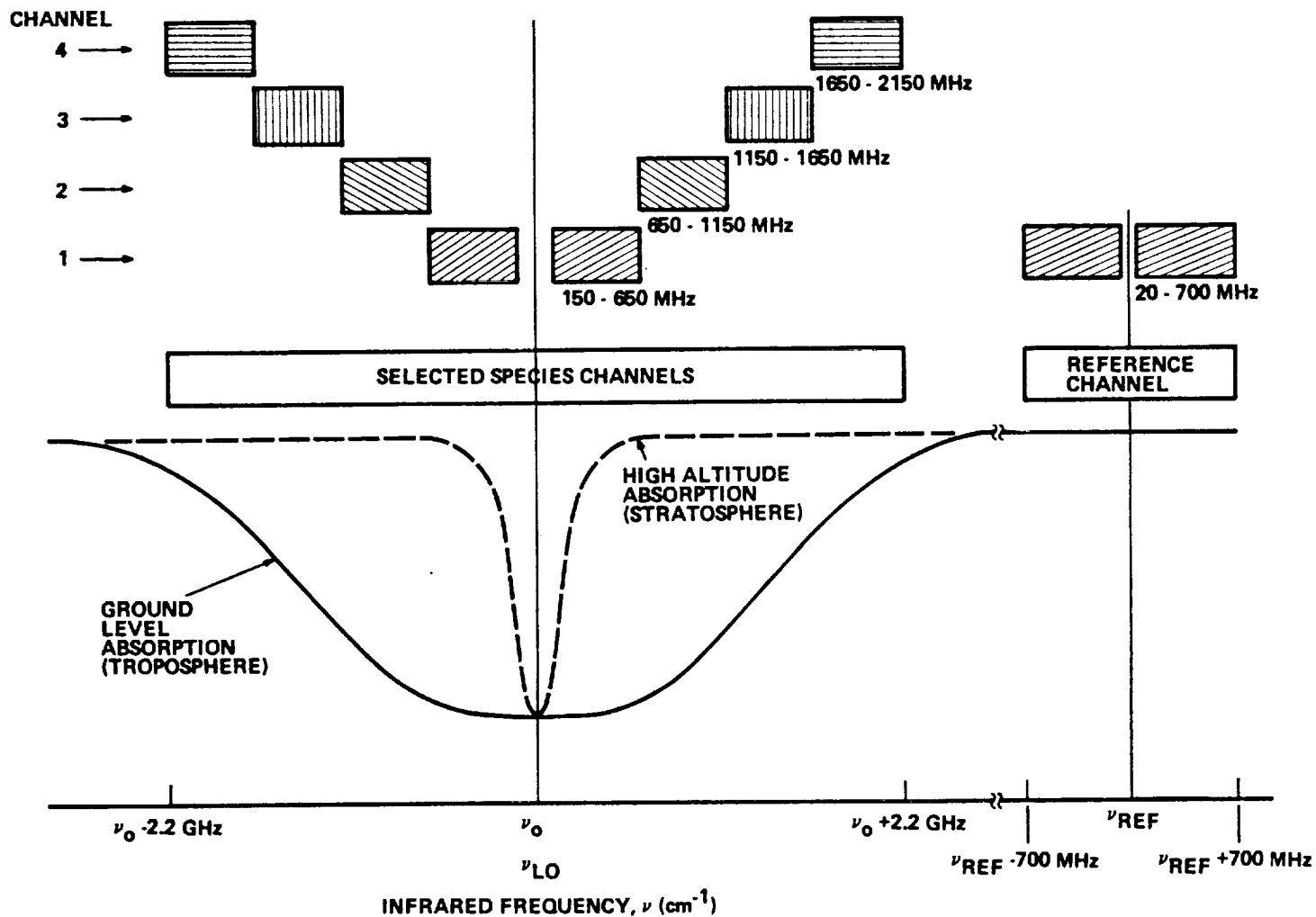
Figure 3-1. Simplified Representation of the Spectral Overlap Between IHR and Absorption Line of Selected Atmospheric Species $(\nu_0 = \nu_{LO})$

15

can provide profiles of the upper troposphere and stratosphere by utilizing a solar occultation (SO) mode in which the sun is viewed tangentially through the various levels of the lower atmosphere during periods of sunrise and sunset.

In the NR measurement mode, the IHR collects the upwelling thermal radiation from the earth and the reradiation from the intervening atmosphere in a spectral region which overlaps the selected vibrational-rotational spectral line. For nadir measurements, the IHR must be mounted on an aircraft, balloon, or satellite platform. Because of the relatively low temperature of the earth, the IHR is sometimes photon starved in the NR mode and is therefore limited by the temperature resolution of the IHR. It has been established that the IHR temperature resolution improves with source black body temperature.[28] Since the sun appears as a black body of approximately 5000 K and the earth appears as a 300 K source, there is a significant difference in the radiance available and the measurement accuracy for the two measurement modes.

In order to demonstrate the feasibility of the IHR remote profiling technique, an aircraft platform was selected to test both operating modes. The dual channel IHR instrument was selected to accompany several other atmospheric constituent measurement instruments on a Latitude Survey Mission of the Pacific Ocean during which SA mode measurements were made at several latitudes and NR measurements were attempted using the upwelling thermal radiance from the earth (ocean).

3.2 INSTRUMENT CONCEPT

The IHR instrument was conceived and developed as a versatile multi-unit system with separate optical package, processing electronics, power supplies, data management, and recording equipment. A simplified block diagram of the IHR system is shown in Figure 3-2.

The IHR optical package is made up of two Dicke-switched, infrared heterodyne radiometer channels which share common receiver optics, FOV, infrared Dicke-switch, and a common calibration technique. In the SA mode, a portion of the incoming solar radiance is made incident on a TV camera which is boresighted with the IHR FOV. A TV monitor with alignment crosshairs allows the operator to manually track the solar image. The partially transmitting mirror is removed, and the tracking unit is bypassed for the NR mode.

The infrared Dicke-switch alternately switches the two radiometer FOV's between the collecting aperture and a reference black body, while supplying a synchronizing signal to the electronic processor. The single
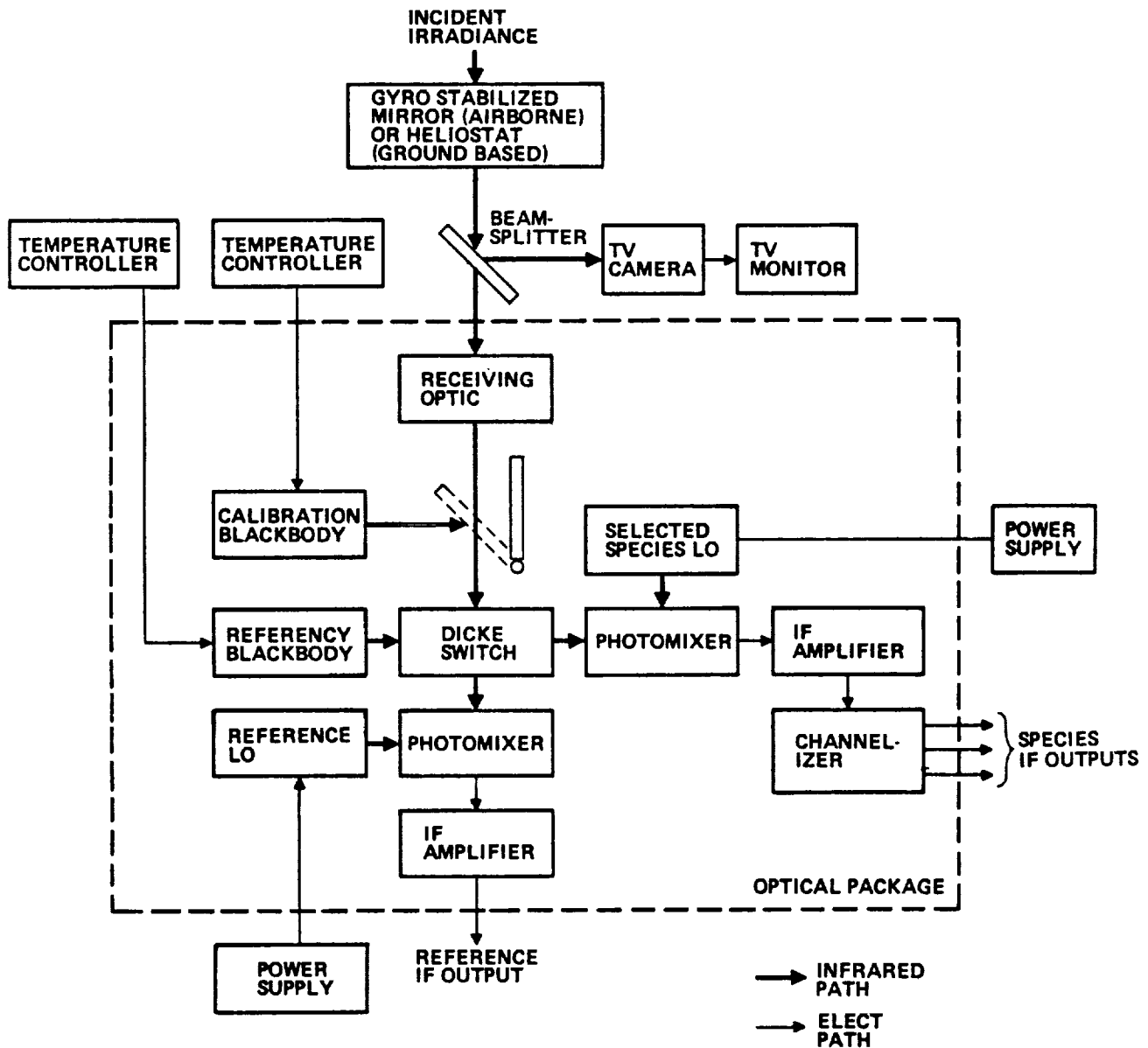
Figure 3-2. Simplified Block Diagram of Dual Laser, Dicke-Switched, IHR Infrared Front-End

17

reference black body, calibration black body, input lens filter, and Dicke-switch are used to provide as many common optical elements for each radiometer receiver as possible, thereby minimizing the errors from separate calibration systems. A calibration black body source is inserted between the collecting aperture and the optical Dicke-switch for IHR calibration. LO power from the two grating tunable CO_2 lasers is optically heterodyned with the source radiance (or the reference radiance) in the photomixers, with the difference IF frequency amplified by wideband IF amplifiers.

Whenever possible, system calibration is carried out at calibration temperatures which are higher and lower than the effective source temperature to allow an accurate determination of the relative source radiance reaching the IHR in each of the four IF channels.

A Dicke-type radiometric signal processor is used when the source and reference temperatures are nearly identical (NR mode). An automatic nulling gain modulation processor is used when the source temperature is much greater than the reference temperature (SA mode).

Some of the advantages of the self-balancing gain modulation processor technique include:

- Greater system stability for high level signals

- Direct digital readout of the postdetection and gain modulating attenuator

- Adaptive integration time constant which provides a long time constant during steady state conditions, and a much shorter effective time constant following a large transient in the effective source radiance.

In order to deal with the large volume of IHR output data, a data acquisition and recording system was designed and constructed which is compatible with the data processing installation at NASA LaRC. Magnetic tape was selected as the mass storage medium for transfer of the field data to the LaRC computer retrieval facility in order to facilitate data reduction. A data management system was incorporated in order to properly format the IHR output data before being recorded on the magnetic tape. The bulk data reduction of the IHR measurement data has been carried out at LaRC. A simplified block diagram of the IHR signal processor and data handling subsystem is shown in Figure 3-3.
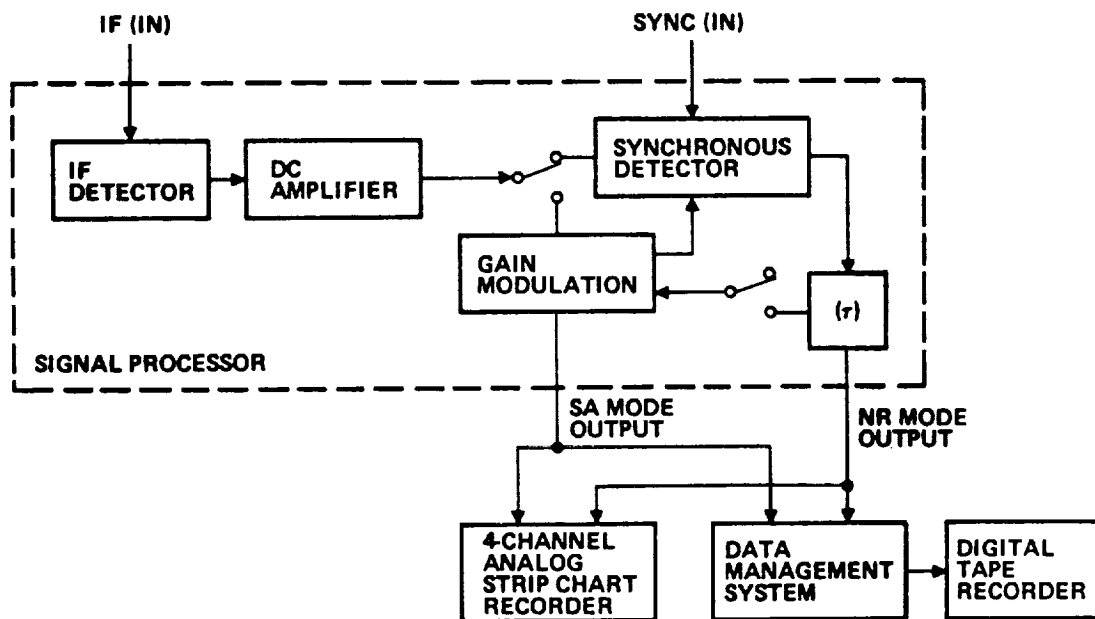
Figure 3-3. Simplified Block Diagram of IHR Signal Processor
and Data Handling Subsystem

19

4.0 IHR CALIBRATION MEASUREMENTS

4.1 IHR TEMPERATURE RESOLUTION

The sensitivity of an IHR can be expressed in terms of its temperature resolution when viewing a thermal source.[27] The exponential increase of black body radiance with temperature prevents the use of a single temperature sensitivity value for all source temperatures. As a result, the theoretical temperature sensitivity expression contains source temperature, T_s, as a variable and is given by:

$$\Delta T_s = \frac{k^2 T_s^2}{2 h^2 \nu^2} \frac{\left(\exp \frac{h\nu}{kT_s} - 1\right)^2}{\alpha \, \exp\left(\frac{h\nu}{kT_s}\right)} \cdot \frac{K}{(B\tau)^{1/2}} \left[\frac{2h\nu\alpha}{k \exp \frac{h\nu}{kT_s} - 1} + \int_{f_1}^{f_2} \frac{NEP(f)\, df}{kB} \right] \quad (4\text{-}1)$$

where:

α = transmission and optical losses between the source and the infrared photomixer

K = sensitivity constant = 2 for Dicke-type receiver

B = predetection bandwidth

τ = postdetection integration time of a true integrator

$NEP(f)$ = heterodyne receiver sensitivity

ν = infrared frequency

k = Boltzmann's constant

h = Planck's constant

f = IF frequency

Equation 4-1 implicitly assumes a polarized source and it must be multiplied by a factor of 2 when an unpolarized thermal source such as the sun or earth is viewed by the IHR.

The heterodyne receiver sensitivity can be expressed in terms of the photon energy, $h\nu$, and the effective receiver quantum efficiency, η', by:

$$NEP(f) = \frac{h\nu}{\eta'} \tag{4-2}$$

where η' is the sensitivity degradation due to impedance mismatches, photo-mixer and preamplifier thermal noise, photomixer frequency response, and insufficient laser LO power. The heterodyne receiver NEP can also be expressed by:

$$NEP = \frac{h\nu}{\eta} \left\{ 1 + \frac{P_{TH}}{P_S} \left[1 + \left(\frac{f}{f_c}\right)^2 \right] \right\} \tag{4-3}$$

where:

η = photomixer quantum efficiency

P_S = photomixer shot noise power

P_{TH} = thermal noise power of photomixer and IF amplifier

f_c = photomixer cutoff frequency

The IHR transmission/optical loss, σ, is made up of several individual component losses as well as the heterodyne mixing efficiency. The calculated optical losses for the IHR is $\sigma \approx 0.34$. The individual component losses are made up of heterodyne efficiency (0.5), telescope transmission (0.98), filter transmission (0.85), Dicke-switch transmission (0.98), beam splitter transmission (0.87), dewar window transmission (0.98), and the $\lambda/4$ plate transmission (0.99).

The IHR temperature resolution is calculated below for an ideal heterodyne receiver which is not limited by the photomixer cutoff frequency, the receiver thermal noise, or the available laser LO power. For $\sigma = 0.34$, $\eta = 0.15$, $\tau = 3$ s, and $\nu = 2.78 \times 10^{13}$ Hz (927.3 cm^{-1}) the calculated temperature resolution for the 680 MHz reference channel (B = 680 MHz) and the 500 MHz species channel (B = 500 MHz) is shown in Figure 4-1. These calculated values of the IHR temperature resolution can be compared with laboratory calibration measurements at $T_s = 500$ K with laser LO wavelengths of

$\nu_R = 920.2$ cm^{-1} and $\nu_S = 927.3$ cm^{-1} for the reference and species channels,

21
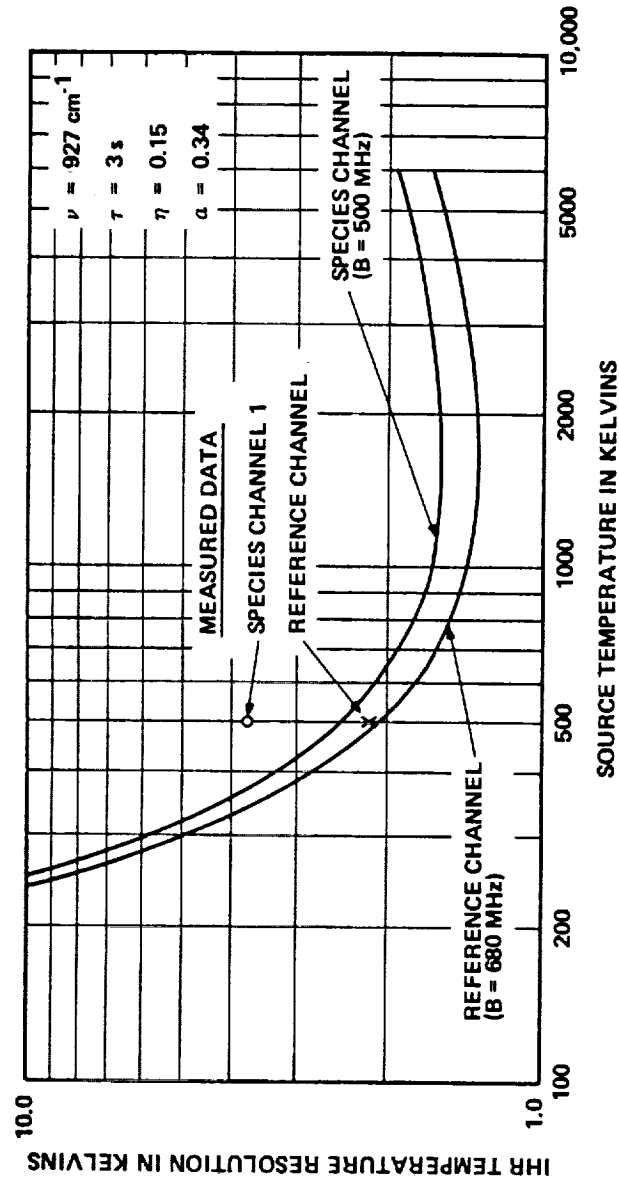
Figure 4-1. Calculated and Measured IHR Temperature Resolution for the Atmospheric Species (NH_3) and Reference Channels

22

respectively. The measured temperature resolution data is given in Table 4-1 for one reference and four species channels.

Table 4-1. Measured IHR Temperature Resolution at 500 K

Reference (20 to 700 MHz)	2.2 K
Species No. 1 (150 to 650 MHz)	3.8 K
Species No. 2 (650 to 1150 MHz)	8.7 K
Species No. 3 (1150 to 1650 MHz)	15.0 K
Species No. 4 (1650 to 2150 MHz)	33.0 K

As can be seen, the measured reference channel temperature resolution of $\Delta T = 2.2$ K is in excellent agreement with the calculated temperature resolution of $\Delta T = 2.1$ K for an effective receiver quantum efficiency of $\eta' = 15$ percent. The effective receiver quantum efficiency value used for the calculation is consistent with the measured photomixer quantum efficiency of $\eta = 19.5$ percent at $\nu = 927$ cm^{-1} and $\nu = 920$ cm^{-1}. The small difference between the measured and calculated effective quantum efficiencies can be attributed to the amplifier thermal noise which was not totally overcome by the photomixer shot noise. Although these temperature resolution measurements were carried out at near $\nu = 927$ cm^{-1} because of the existence of a suitable ammonia absorption line, it should be noted that the maximum reference channel photomixer quantum efficiency of $\eta = 30$ percent occurs near $\nu = 985$ cm^{-1} ($\lambda = 10.15$ μm). The use of this photomixer in the IHR permitted atmospheric profiling measurements near both 10.8 μm (ammonia species) and 9.6 μm (ozone species). In a dedicated experiment, the photomixer would be selected for the particular spectral region of interest.

The measured temperature resolution in the species No. 1 (150 to 650 MHz) channel of the IHR is $\Delta T = 3.8$ K and corresponds to an effective receiver quantum efficiency of $\eta' = 10$ percent at $\nu = 927$ cm^{-1}. The effective receiver quantum efficiency is in good agreement with the measured

23

photomixer quantum efficiency of η = 15 percent. As can be seen in Figure 4-1, the calculated and measured IHR temperature resolution for the species No. 1 channel are in good agreement.

As can be seen from Table 4-1, the higher frequency species channels exhibit a significantly degraded temperature resolution compared to the reference and species No. 1 channel. Based upon the species channel measured temperature resolution, an effective photomixer 3-dB cutoff frequency of approximately 550 MHz was calculated. For this particular photomixer in the species channel, the roll-off in the IHR temperature resolution with increasing IF frequencies as inferred from the measurement data, is much faster than can be explained based on the measured roll-off of the photomixer frequency response. The measured frequency response of the reference and species photomixers is shown in Figure 4-2. It can be seen that the reference photomixer has a 3-dB cutoff frequency of $f_c \approx$ 650 MHz and the species photomixer has a 3-dB cutoff frequency of $f_c \approx$ 1200 MHz.

Based on the IHR temperature resolution measurement data, it is postulated that: (1) the IF preamplifier which is mounted in the species dewar may exhibit higher thermal noise than expected at the higher IF frequencies due to a poor impedance match between the photomixer and the preamplifier input and (2) as anomaly exists in the shot noise spectrum as exhibited by this particular type of photomixer.

It should be noted that the species channel photomixer was also chosen to have a spectral response characteristic which permitted efficient (but not optimum) heterodyne receiver operation at both λ = 10.8 μm (ammonia) and λ = 9.6 μm (ozone). The species channel photomixer exhibits a peak quantum efficiency of $\approx$30 percent near $\nu \approx$ 1000 cm^{-1} ($\lambda \approx$ 10 μm).

4.2 IHR MEASUREMENT LINEARITY

A variable temperature, external black body source was used to simultaneously measure the linearity of each of the IHR channels. The IHR linearity is extremely important because calibration measurements are usually carried out at temperatures widely separated from the "effective" source temperature. The linearity of the IHR can be one of the limitations of the overall accuracy of the IHR measurement data.

The external black body output was collected by a 6-inch diameter off-axis paraboloid and collimated. This collimated black body radiance was then aligned with the input optic of the IHR. The digital output of the four electronic processors operating in the GAIN MOD mode was then recorded as the black body source temperature was varied between 300 K and 1273 K. The digital output of each channel is displayed on the front

24

panel of each of the processors as an integer between 0 and 1023. The range and resolution settings of the individual processors are set independently based upon the IHR temperature resolution in the particular IF channel. As a result, the measured linearity curves (Figures 4-3 through 4-6) for the four channels show fewer offset counts for the 1000 K temperature range as the center frequency of the IF channel increases. This corresponds closely to the observed degradation of temperature resolution with increasing IF frequency.

Each of the four channels, one reference and three species, can be seen to exhibit excellent linearity over the measurement temperature range. Each of the channels shows approximately the same pattern of small deviations from the best-fit linear curve. For example, the 300 K and 1300 K points are consistently higher than expected and several of the other points are consistently lower than expected. Although the two radiometers and their IF channels are independent, it can be seen that the small deviation patterns of the linearity measurements match. It is anticipated that this systematic deviation can be attributed not to an imperfection in the IHR, but to an imperfect calibration of the black body. The deviation of the IHR outputs from linearity can be considered to be very small, with the reference channel showing a deviation of much less than 1 percent.
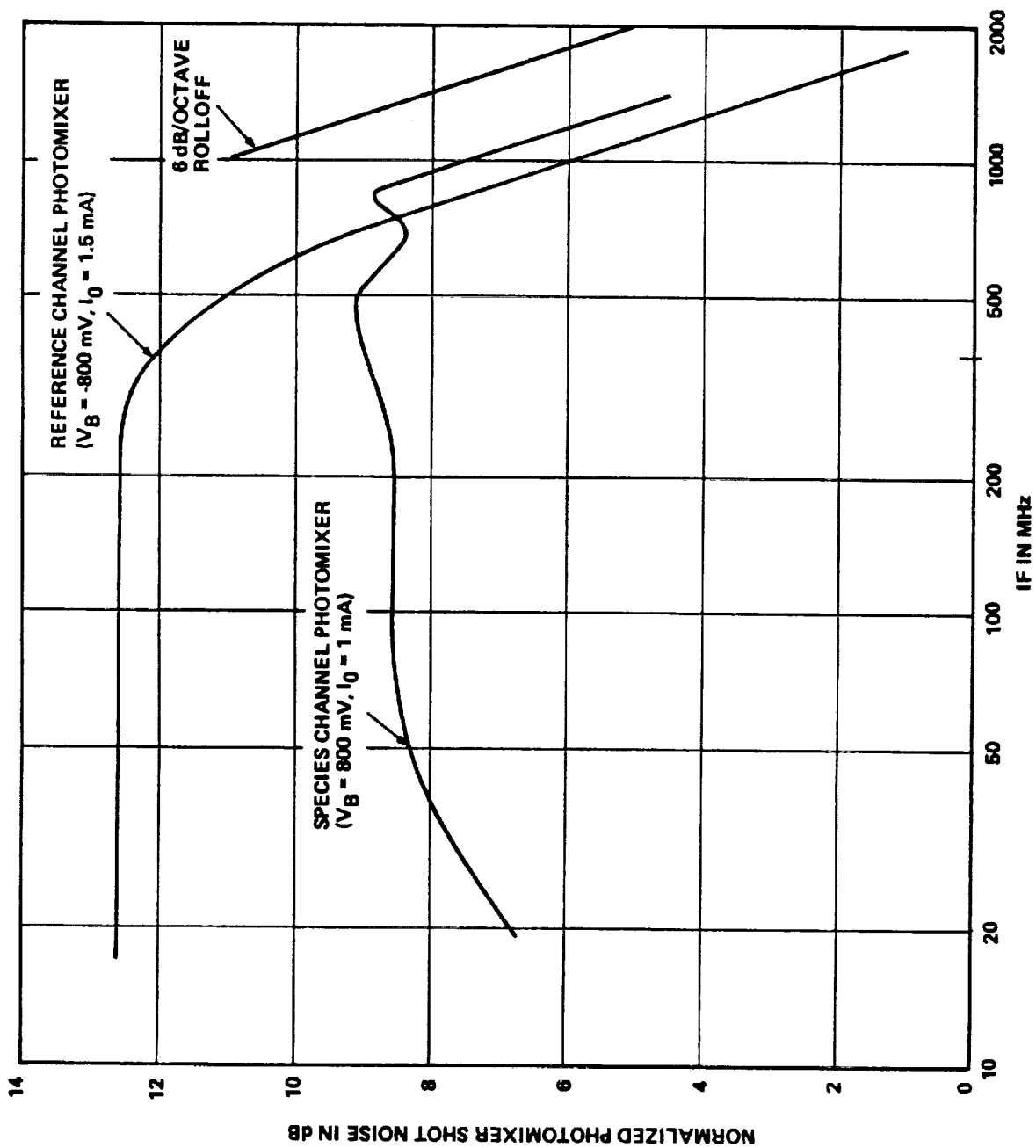
Figure 4-2. Measured PV:HgCdTe Photomixer Frequency Response of IHR

26
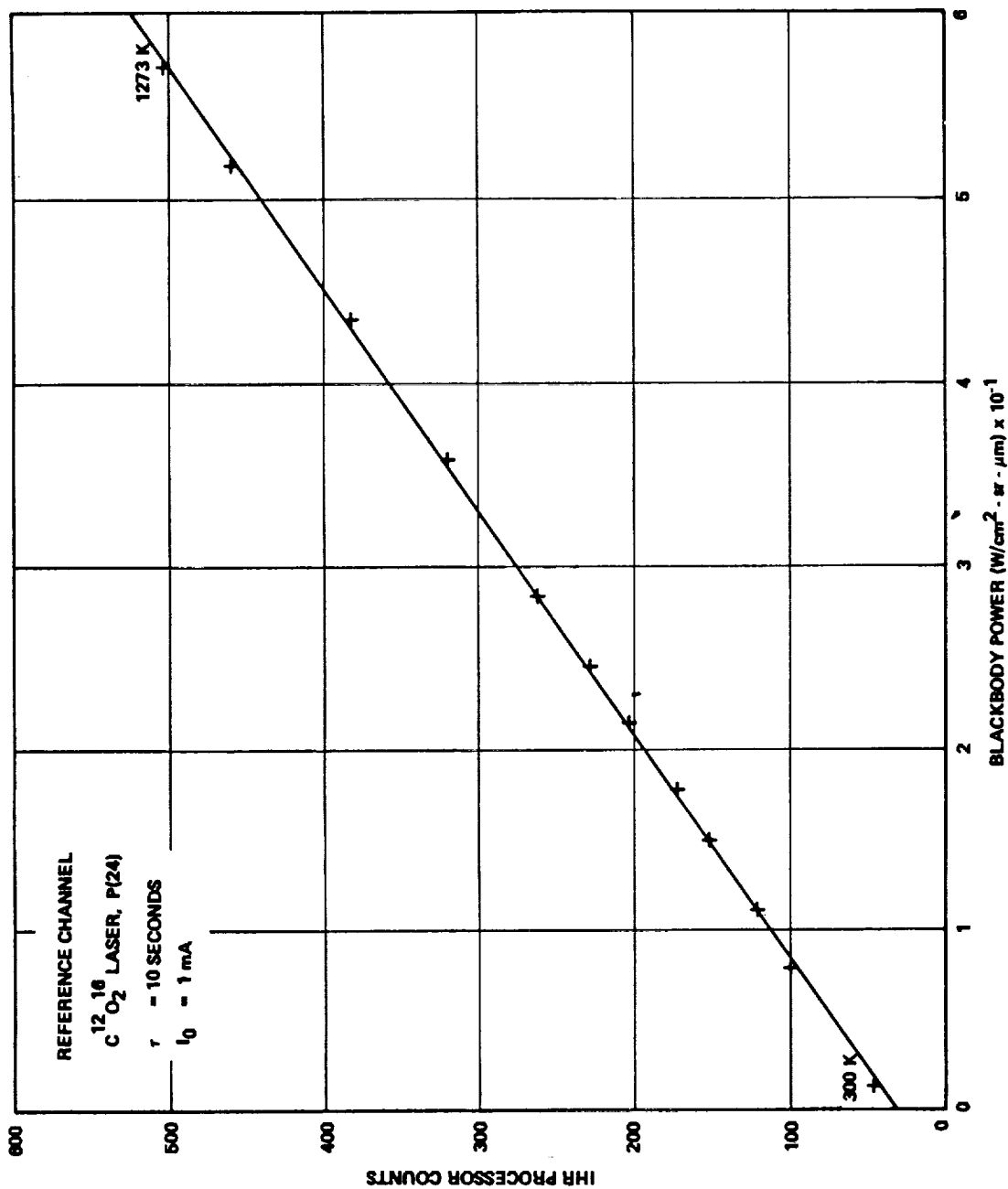
Figure 4-3. Measured Linearity of IHR Reference Channel for 360-MHz IF Center Frequency

27
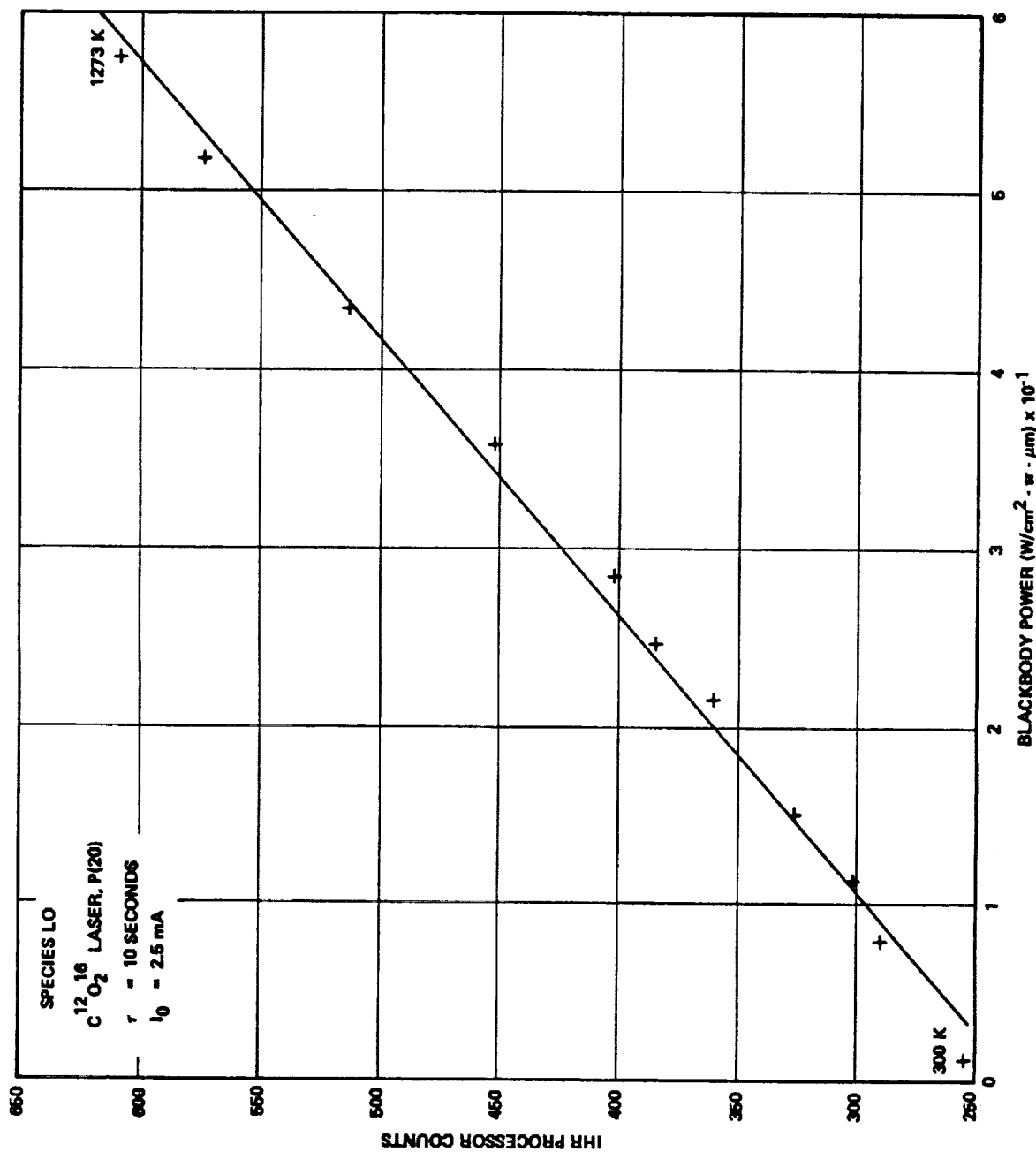
Figure 4-4. Measured Linearity of Species Channel for 400-MHz IF Center Frequency
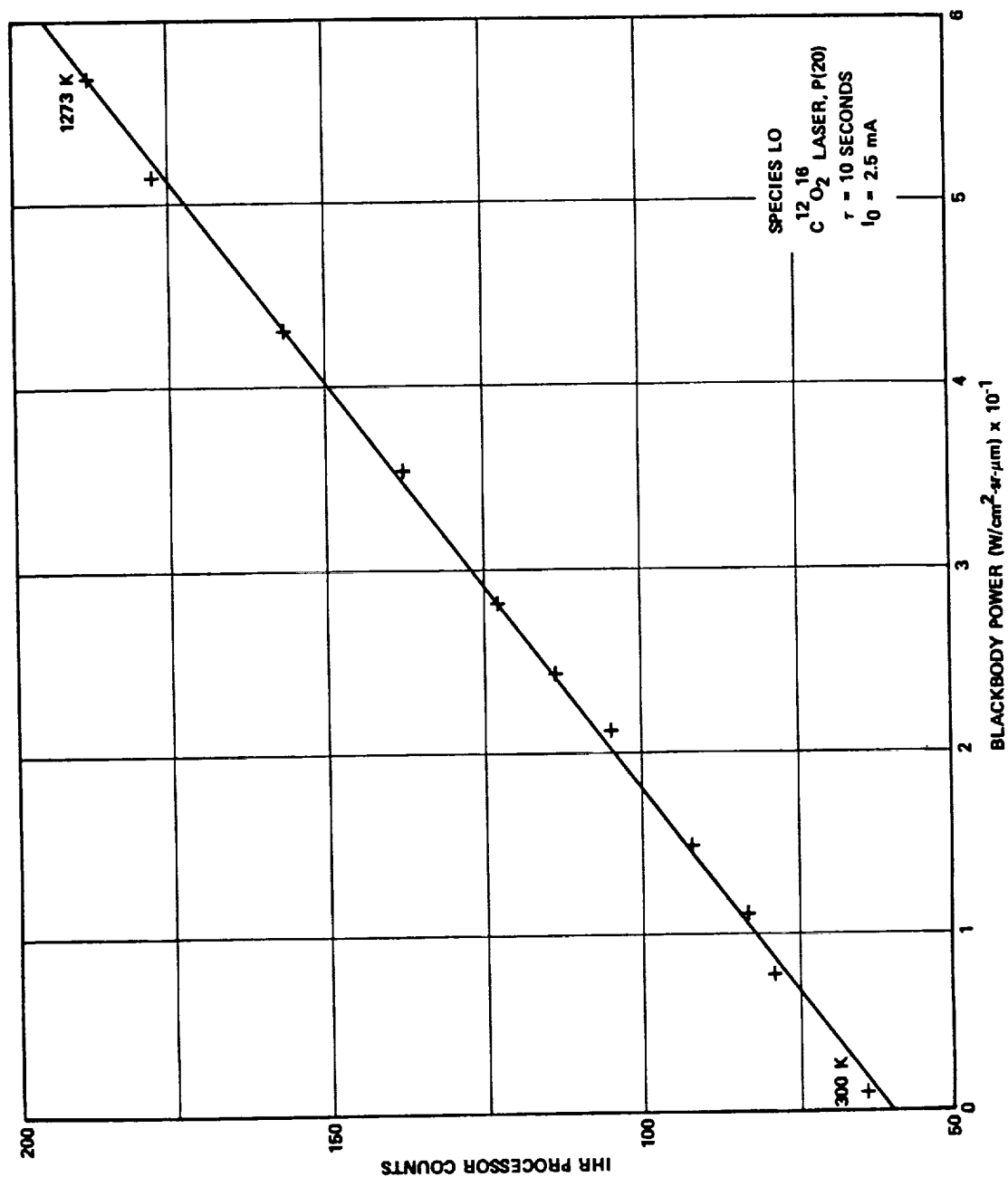
Figure 4-5. Measured Linearity of Species Channel for 1400-MHz IF Center Frequency
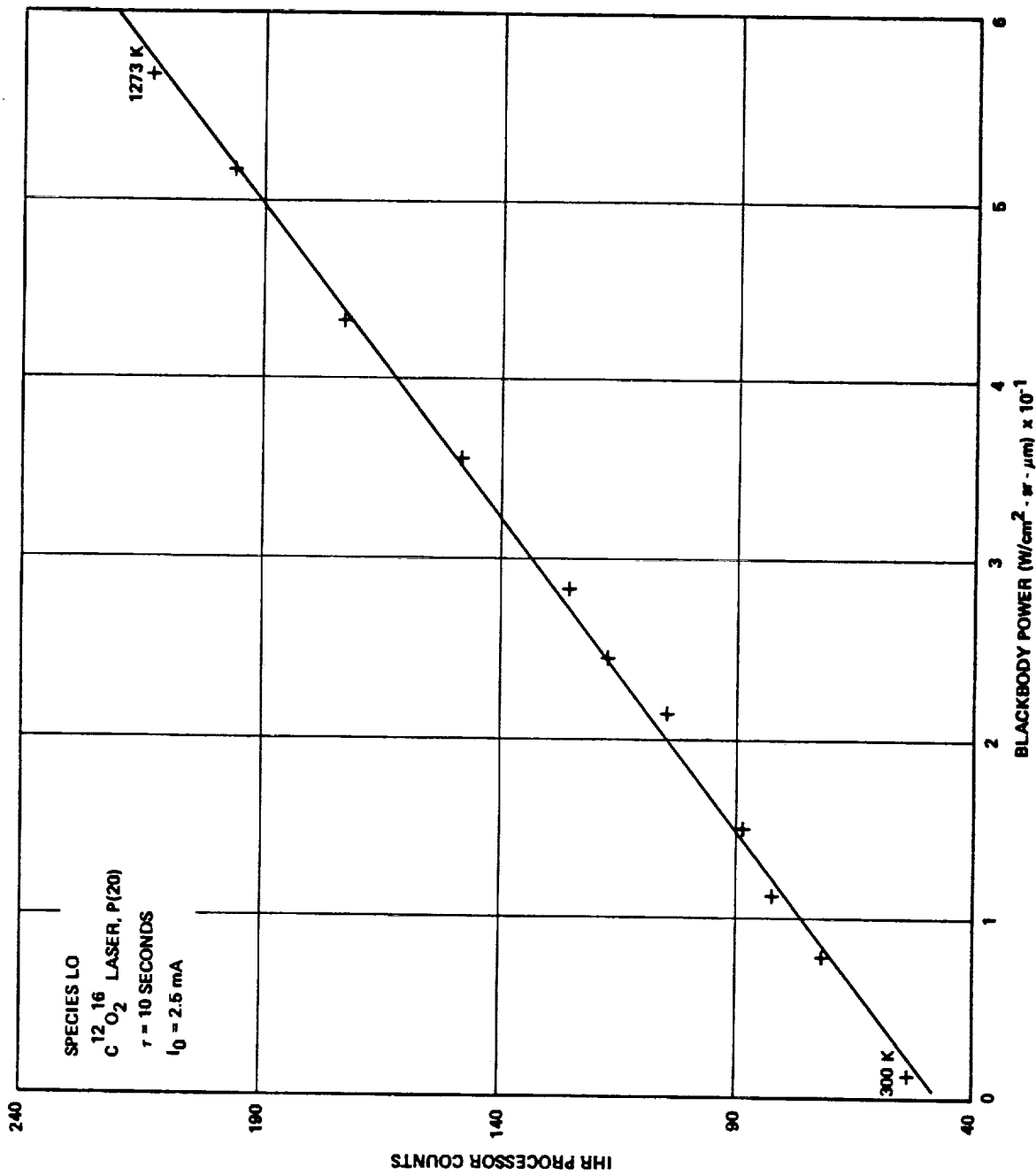
Figure 4-6. Measured Linearity of Species Channel for 1900-MHz IF Center Frequency

5.0 ATMOSPHERIC ABSORPTION MEASUREMENTS
AND REMOTE AMMONIA PROFILING

5.1 ATMOSPHERIC ABSORPTION MEASUREMENTS

The IHR was used to make narrowband atmospheric transmission measurements at several selected isotopic CO_2 laser wavelengths. The CO_2 isotope was $C^{13}O_2^{16}$ which has an atmospheric concentration approximately two orders of magnitude below the atmospheric concentration of the normal isotope $C^{12}O_2^{16}$. Therefore, the use of $C^{13}O_2^{16}$ laser local oscillators results in a higher overall atmospheric transmittance.

Atmospheric absorption measurements were carried out using the sun as a back-lighting source. The solar radiation was tracked and directed onto the input telescope of the IHR by means of a roof mounted heliostat. The heliostat consisted of a pair of mirrors, one of which was attached to a clock-motor-driven equatorial mount. This arrangement allowed the solar energy to be brought into the solar tracking laboratory at AIL in a fixed position which is independent of solar zenith angle.

As the solar radiation passes through the atmosphere it is selectively absorbed by the various atmospheric constituents. The number of absorbing molecules in the atmosphere between an observer on the ground and the sun, neglecting refraction, is given by:

$$\int N_h \, dL \qquad (5\text{-}1)$$

where:

N_h = number of absorbing molecules per unit volume at altitude h

L = slant height

31

The increment of path length, dL, is given by:[29]

$$dL = \frac{1 + h/R}{\left(\cos^2 \theta_z + \frac{2h}{R} + \frac{h^2}{R^2}\right)} \; 1/2 \; dh \qquad (5\text{-}2)$$

where:

θ_z = solar zenith angle

R = radius of the earth

In the plane-parallel approximation for the earth's atmosphere, the denominator of equation 5-2 is dominated by the first term so that equation 5-2 can be reduced to:

$$dL = \sec \theta_z \; dh \qquad (5\text{-}3)$$

This approximation is valid in general for zenith angles of less than 85 degrees. It is also valid for low-altitude atmospheric layers which are close to the horizon.

The absorption, α, produced by a length, L, of an optically thin gas is given by:

$$\alpha = \exp \left[\beta(\nu) L \right] \qquad (5\text{-}4)$$

where $\beta(\nu)$, the absorption coefficient, is shown as an explicit function of frequency.

Equation 5-4 can now be rewritten in terms of transmission through the gas as:

$$\tau = 1/2 \exp \left[-\beta(\nu) L \right] \qquad (5\text{-}5)$$

This general equation holds because the transmissivity of the atmosphere at $C^{13}O_2^{16}$ wavelengths is primarily dependent upon the water vapor continuum,

particulate matter, and the $C^{13}O_2^{16}$ itself. Combining equations 5-3 and 5-5 yields:

$$\tau = \exp\left[-\beta(\nu)\,h\,\sec\,\theta_z\right] \qquad (5\text{-}6)$$

Taking the natural logarithm of both sides of equation 5-6 yields a linear relationship between log τ and sec θ_z.

Figure 5-1 shows a typical atmospheric transmission measurement performed by the IHR at the R(16) and R(18) transitions of the $C^{13}O_2^{16}$ laser. The R(16) data was obtained using the reference channel detector and electronics, while the R(18) data used the 400-MHz species channel detector and electronics. The linear relationship predicted by equation 5-6 is readily apparent in the measurement data. The relatively large scatter of the points is believed to be caused primarily by atmospheric fluctuations. The lines in Figure 5-1 were computer generated using linear regression. While a definitive calculation of the atmospheric absorption coefficients requires a great deal of coordination with water vapor measurement data, some approximate values can be determined using the measured data. The slopes of the lines in Figure 5-1 are the products of the absorption coefficients and the atmosphere's vertical height since:

$$\ln\,\tau = -\beta(\nu)\,h\,\sec\,\theta_z \qquad (5\text{-}7)$$

The zenith transmission, τ_z, can then be obtained from equation 5-7 for sec $\theta_z = 1$:

$$\tau_z = \exp\left[-\beta(\nu)\,h\right] \qquad (5\text{-}8)$$

Table 5-1 gives the atmospheric attenuation coefficient, $\beta(\nu)h$, and the resultant atmospheric transmission, τ_z, at the zenith for the three $C^{13}O_2^{16}$ transitions measured; R(14), R(16), and R(18). These values are higher than those previously measured ($\tau_z = 0.59$)[27] as would be expected from the fact that these measurements are at the rare isotope $C^{13}O_2^{16}$ wavelengths while the earlier measurements were made at wavelengths about the more abundant natural isotope $C^{12}O_2^{16}$.

33
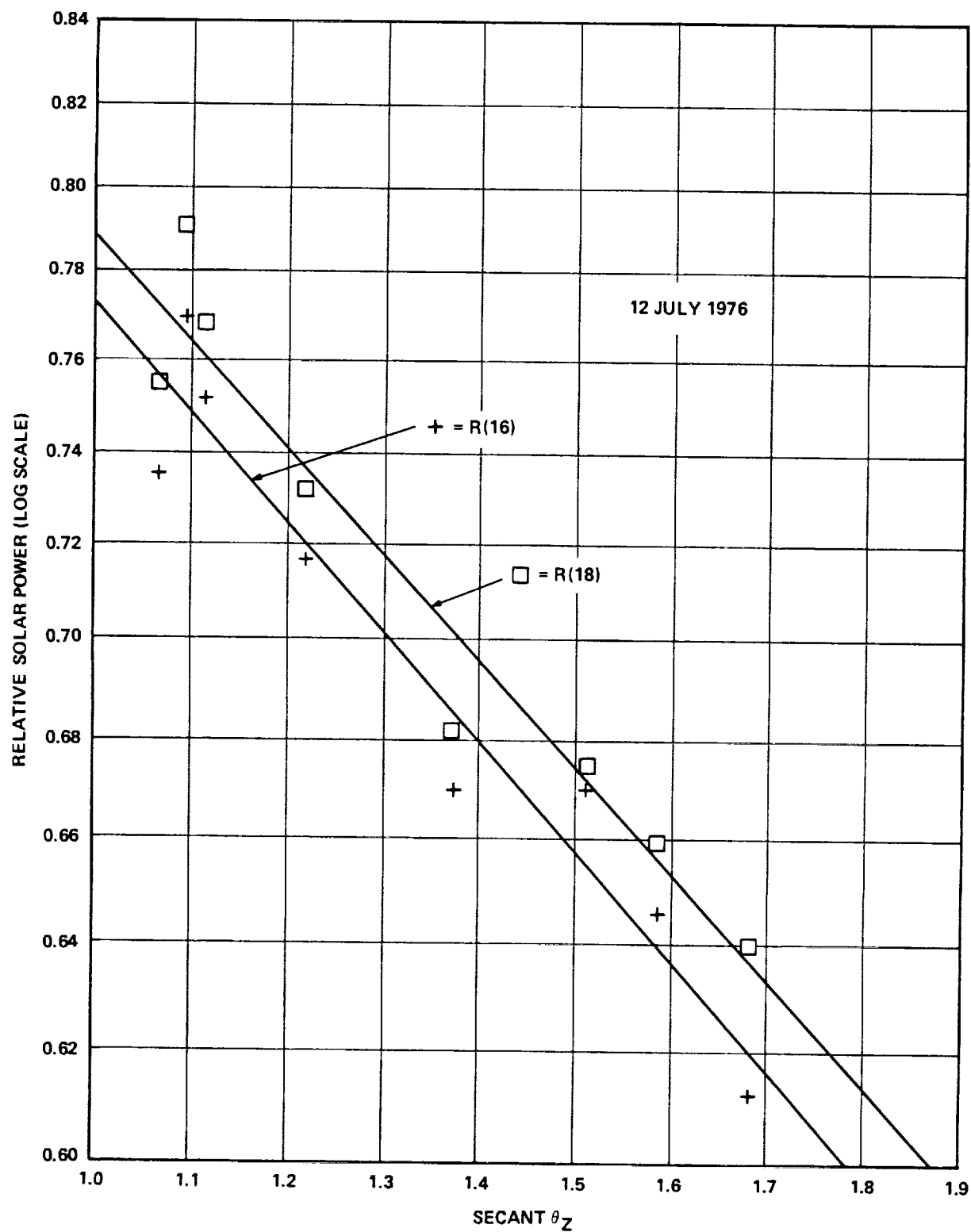
Figure 5-1. Measured Atmospheric Transmissivity at R(16) and R(18)
Transitions of $C^{13}O_2^{16}$ Laser

34

Table 5-1. Measured Atmospheric Transmission at Selected
Wavelengths Around $C^{13}O_2^{16}$ Laser Transitions

$C^{13}O_2^{16}$ Laser Line	IF Center Frequency	$\beta(\nu)h$	τ_z (Zenith Atmospheric Transmission)
R(14)	± 360 MHz	0.312	0.732**
R(16)	± 360 MHz	0.323	0.724*
R(18)	± 400 MHz	0.314 0.260	0.731* 0.771**
R(18)	±1400 MHz	0.341 0.272	0.711* 0.762**
R(18)	±1900 MHz	0.320 0.185	0.726* 0.831**

R(14) at ν_0 (924.5276 cm^{-1})

R(16) at ν_0 (925.9240 cm^{-1})

R(18) at ν_0 (927.3004 cm^{-1})

* 12 July 1976

** 18 August 1976

It can be inferred from Table 5-1 that atmospheric conditions were somewhat different for the 2 days of measurements. Comparison of the absorption coefficients measured at the R(18) transition shows a variation of approximately 20 percent along with commensurate differences in the zenith transmissivity. This measurement scatter is expected to be caused by fluctuations in the relative humidity and aerosol content of the atmosphere over the relatively long measurement time (≈ 4 hours).

5.2 REMOTE AMMONIA PROFILING

The IHR was used to obtain remote vertical profile measurements of tropospheric ammonia. The ammonia weighting functions used for the ground-based SA mode measurements are shown in Figure 5-2. Measured ammonia concentrations using these weighting functions are given in Figures 5-3, 5-4, and 5-5 and are believed to be the first remote ammonia profile measurements.

20

18

16

14

WEIGHTING FUNCTIONS

NH_3 (927.308 cm^{-1})

ALTITUDE km

12

$\tau = 10\ s,\ B = 500\ MHz$

$\delta f_1 = \pm 1900\ MHz$

10

$\delta f_2 = \pm 1400\ MHz$

$\delta f_3 = \pm 900\ MHz$

8

$\delta f_4 = \pm 400\ MHz$

6

4

2

0

0   0.2   0.4   0.6   0.8   1.0   1.2

NORMALIZED WEIGHTING FUNCTION

δf_4

δf_3

δf_2

δf_1
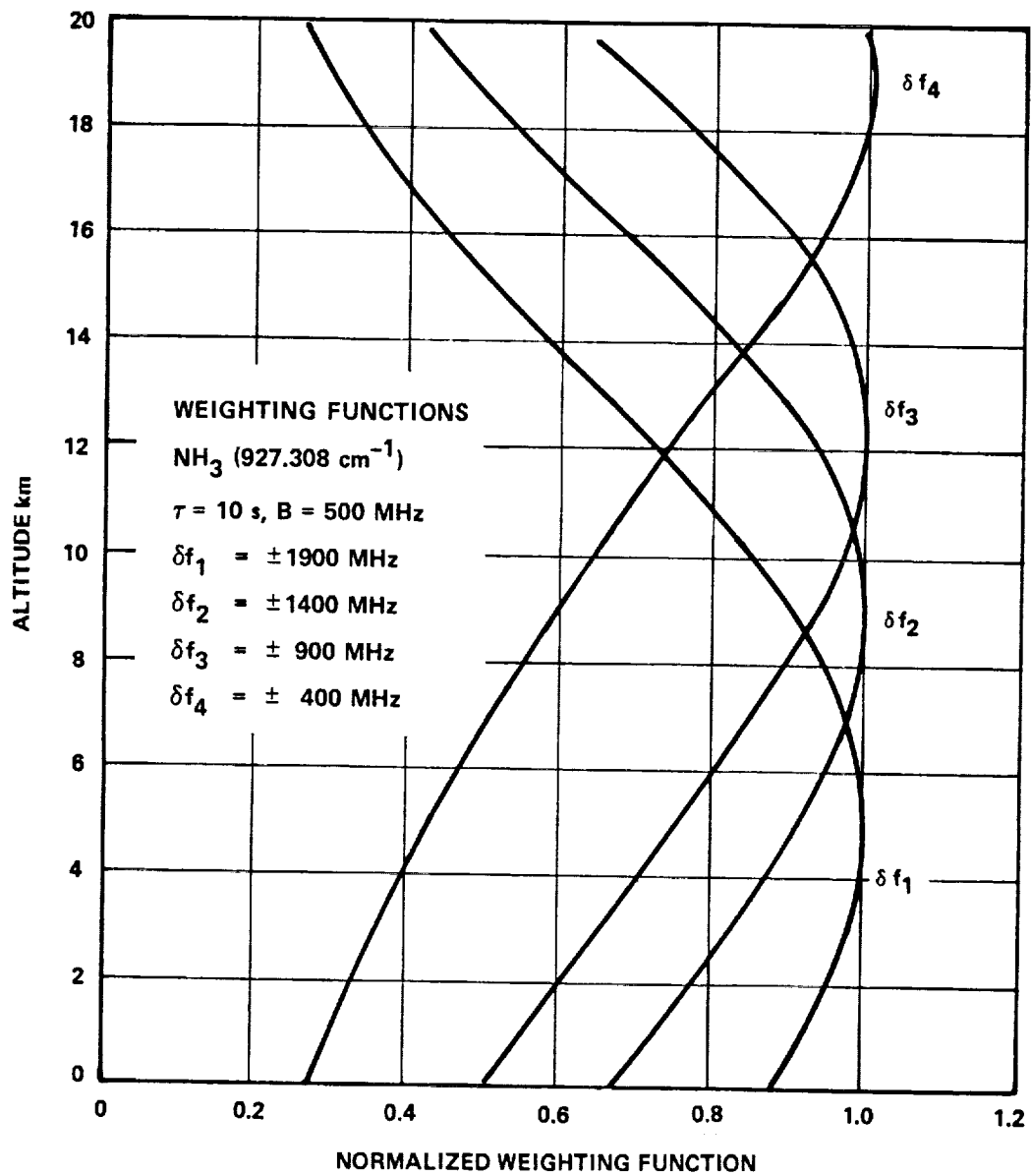
Figure 5-2. Ammonia Weighting Functions (SA Mode)

36

SPECIES: $C^{13}O_2^{16}$ R(18) ±1900, ±1400, ±400 MHz

REF: $C^{13}O_2^{16}$ R(8) ±360 MHz

18 MARCH 1976
INITIAL GUESS: 25 ppbV

ALTITUDE IN km

NH₃ CONCENTRATION IN ppbV
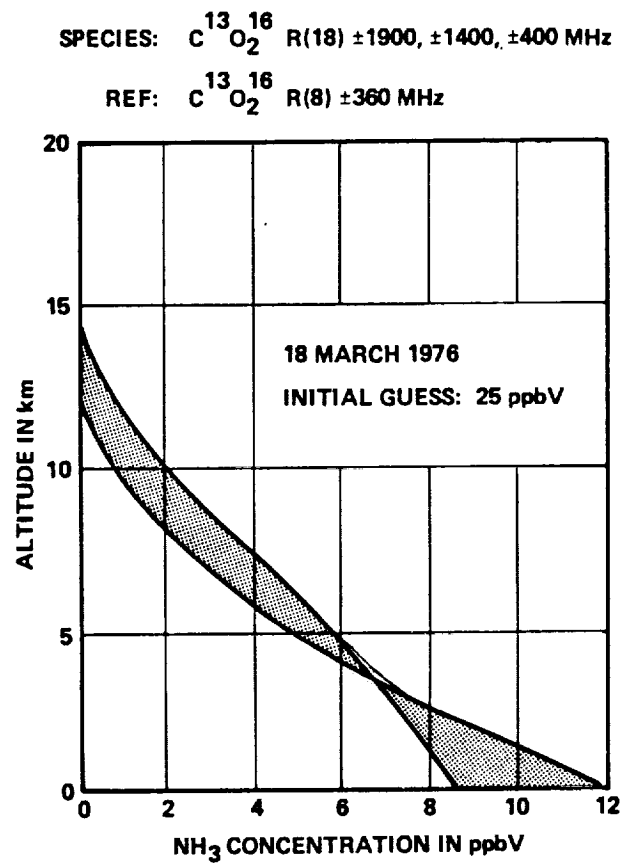
Figure 5-3. Measured Ammonia Profile Using Independent Reference Channel

37
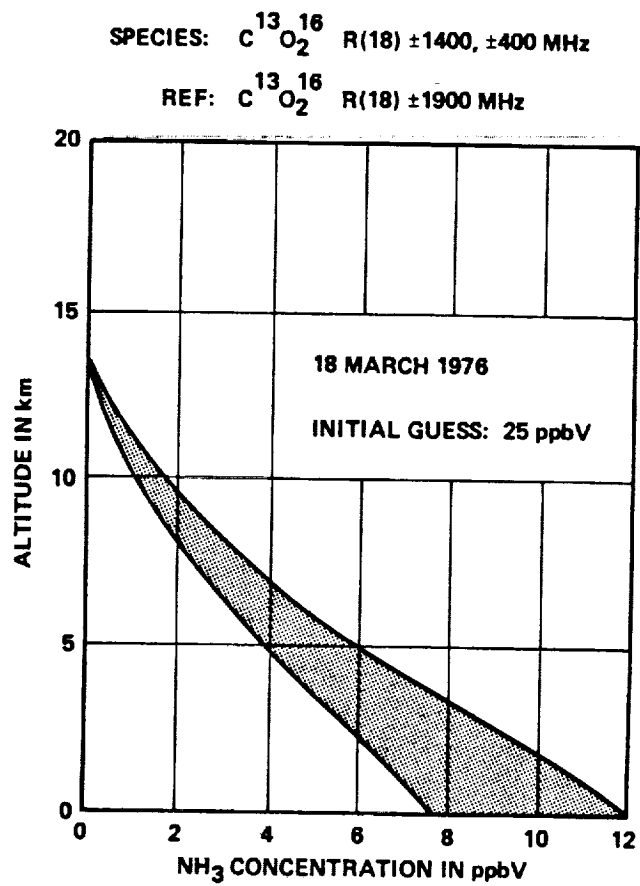
Figure 5-4. Measured Ammonia Profile Using 1900-MHz IF Center Frequency Species Channel as Reference

SPECIES: $C^{13}O_2^{16}$ R(18) ±1900, ±1400, ±400 MHz

REF: $C^{13}O_2^{16}$ R(8) ±360 MHz

INITIAL GUESS: 25 ppbV
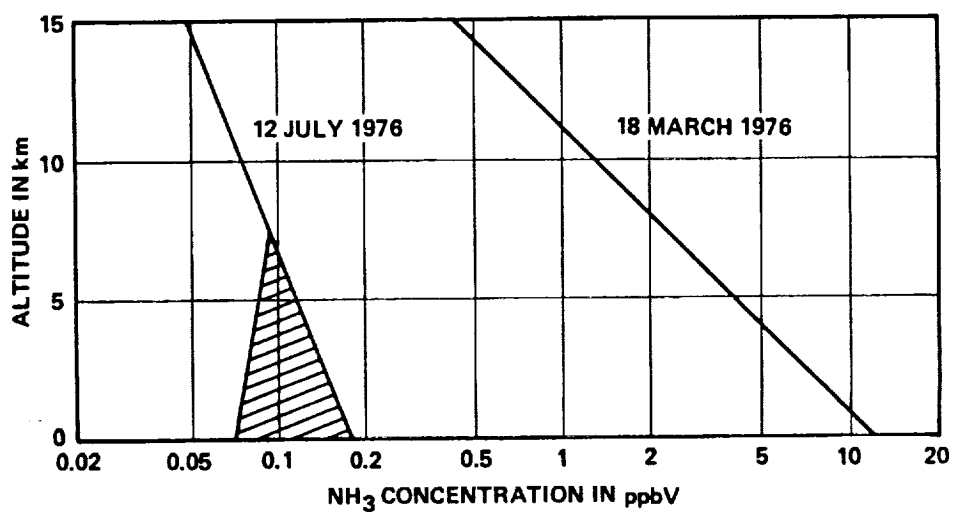
Figure 5-5. Comparison of Measured Ammonia Profiles in Spring and Summer of 1976

39

Figures 5-3 and 5-4 indicate measured NH_3 concentrations of 8 to 12 ppbv near ground level and decreasing through the troposphere to less than 1 ppbv above an altitude of 10 km. These measurements were taken at AIL, Melville, New York on 18 March 1976. The IHR pollutant and reference channel lasers were operating on the R(18) and R(8) transitions of the $C^{13}O_2^{16}$ laser at ν = 927.300 cm^{-1} and ν = 920.219 cm^{-1}, respectively.

The ammonia profiles shown in Figures 5-3, 5-4, and 5-5 were derived from measured radiances in the IHR channels by means of an iterative inversion procedure.[28] Vertical temperature profile data was obtained from radiosonde measurements taken at Fort Totten, Queens, New York, and spectroscopic data[25] combined with recent experimental measurements of ammonia absorption coefficients[26] were used to provide the absorption coefficients for the inversion calculations. An initial guess profile of a constant 25 ppbv was used to initiate the inversion procedure. However, the results were not sensitive to the choice of initial guess.

Ammonia is produced by natural organic breakdown and is a by-product in the organic chemical industry, domestic incinerators, and automobile exhausts. As a result, NH_3 is frequently found in urban atmospheres. Although disagreement exists regarding the concentration and vertical distributions of atmospheric NH_3, concentrations are generally expected to be between 5 and 20 ppbv near ground level with decreasing concentration through the troposphere to sub-ppbv levels in the stratosphere.[18,19] The measured NH_3 data are in good agreement with these expected values.

The retrieved data shown in Figures 5-3 and 5-4 show the effects of the reference channel on the data retrievals. In Figure 5-3, the three R(18) pollutant channels are used as indicators of NH_3 concentration at different altitudes and are referenced to the R(8) clear reference channel. This method provides the maximum NH_3 discrimination and profiling with the possible uncertainty of absorption by unknown gases in the reference channel. In Figure 5-4, two of the R(18) channels have been used as pollutant indicators. They are referenced to the third R(18) channel which is located in the wings of the selected NH_3 absorption line. This provides a spectrally closer reference channel at the expense of some profiling information. In both cases, the general trend of results is consistent, which indicates that the R(8) clear channel provides a good reference.

Although the IHR measurements in March 1976 indicated a ground level ammonia concentration of about 10 ppbv, IHR measurements in July 1976 resulted in ground level concentrations near 0.2 ppbv (Fig-5-5). The lower ammonia concentration is believed to be due to the seasonally higher atmospheric water vapor concentration that was experienced during early July 1976.[19] The error bars in the July 1976 retrieval data are due to the lower measured ammonia concentration and the relatively lower sensitivity in the 1900-MHz low altitude channel.

6.0 IHR AIRBORNE MEASUREMENTS

6.1 STRATOSPHERIC OZONE MEASUREMENTS

Stratospheric ozone measurements were performed over a wide range of latitudes using the NASA CV-990 airborne laboratory. For measurements in the SA mode, the IHR was operated in the GAIN MOD mode using the sun as a radiant source. Airborne solar observations were conducted for up to 60 minutes per day. Whenever possible, IHR calibrations were carried out at calibration temperatures which were larger and smaller than the "effective" temperature of the source to allow an accurate determination of the relative solar energy reaching the IHR in each of the four IF spectral channels (three species and one reference). The IHR was calibrated at 5-minute intervals during the solar measurement periods. As a result, ozone measurements on up to three separate species lines were possible during any 60 minute measurement period.

Retrieved ozone profiles, obtained between 18°N and 56°N latitude, exhibited a shift in the altitude of the peak ozone concentration from 16 km at 56°N to 20 km at 18°N latitude. This trend is in general agreement with the seasonally averaged ozone distributions from chemical balloon soundings at 10°N and 60°N as shown in Figure 6-1.

The profiles obtained on the Latitude Survey Flight Mission clearly demonstrate that remote profile concentrations of atmospheric species, such as ozone, can be obtained utilizing the IHR. Unfortunately, corroboration of the measured ozone profiles with ground truth data was not possible during the Latitude Survey Mission; ground truth data was available on the following series of IHR airborne measurements which were conducted during the "ASSESS II" Mission in May 1977.

A typical retrieved ozone profile measured by the IHR during the second flight mission is shown in Figure 6-2. Figure 6-2 includes a directly measured ozonesonde profile* that was obtained on the previous day in the same geographic area as the IHR measurement. An excellent correlation can be seen between these two coordinated ozone measurements.

---

* Ozonesonde measurements were carried out over a period of 7 consecutive days. The balloons were released from San Diego, California; Great Falls, Montana; and Denver, Colorado. The measured ozone profiles exhibited very little variations over the 7-day period.
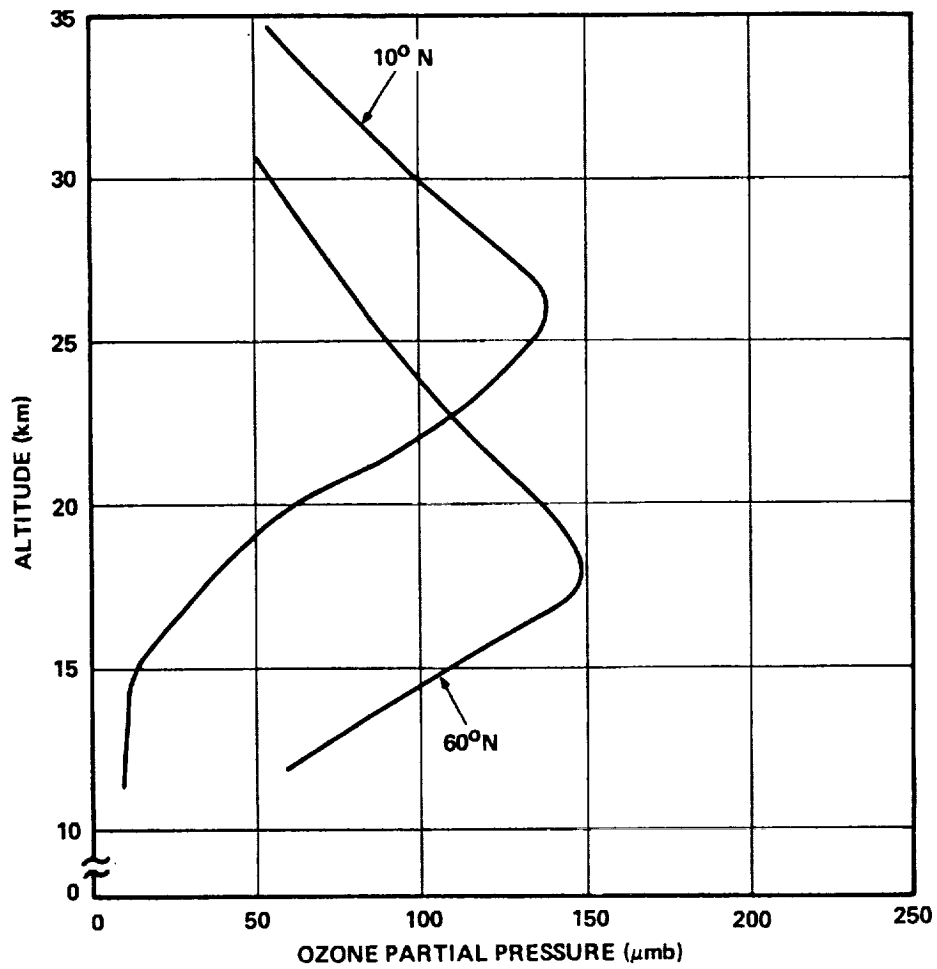
Figure 6-1. Seasonally Averaged Ozone Distribution from Chemical Balloon Soundings at Two Selected Latitudes

43
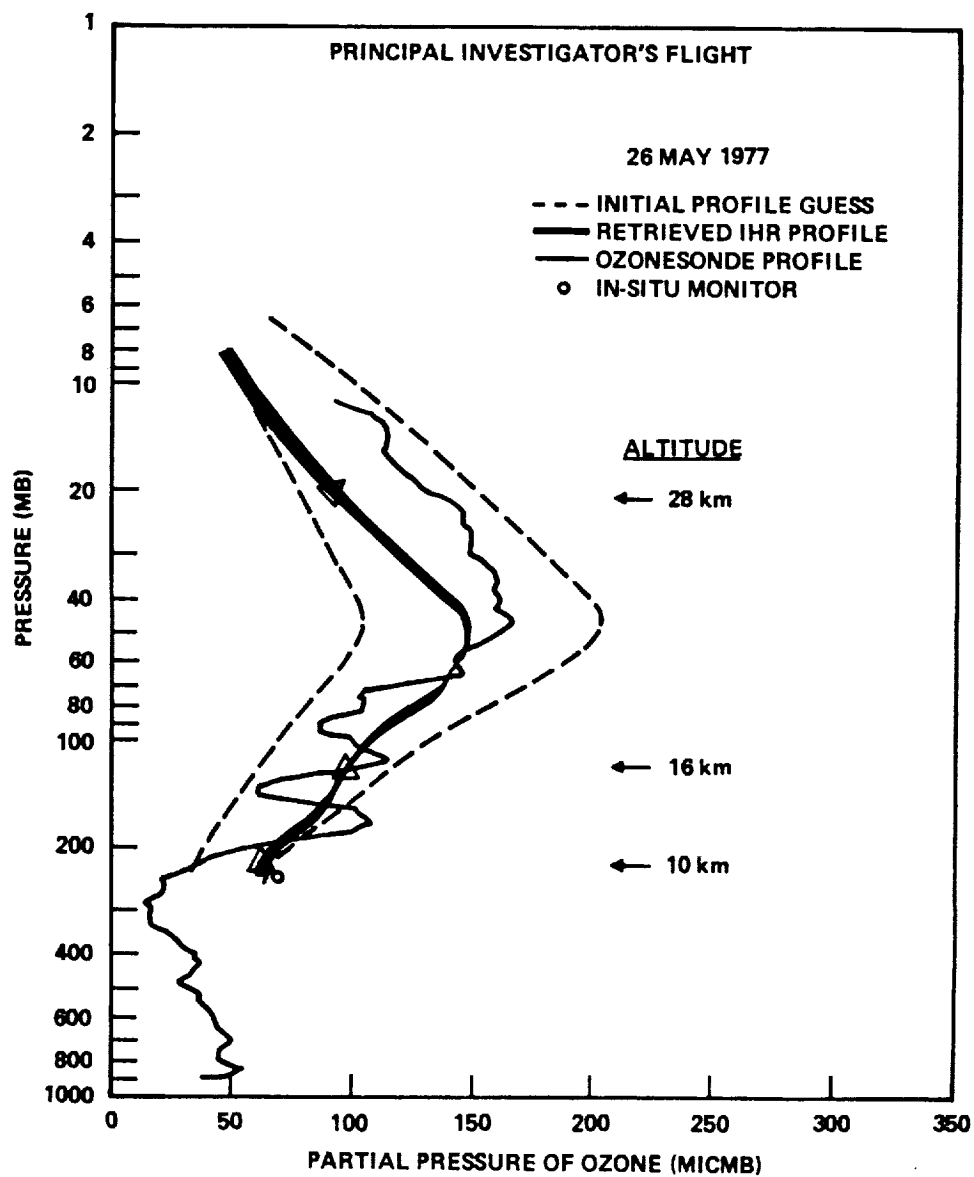
Figure 6-2. IHR Retrieved Ozone Profile Including Ground Truth Balloon and Aircraft In Situ Measurement Data

An additional piece of ozone ground truth data was obtained from an insitu gas sampling instrument aboard the CV-990. The instrument was a gas sampling, self-contained ultra-violet absorption photometer developed by NASA Lewis Research Center as part of NASA's GASP Program. At the time of the IHR profile measurement, the insitu instrument measured an ozone partial pressure of 71 MICMB which is in excellent agreement with the 60 to 65 MICMB value obtained from the IHR retrieval.

The total ozone burden obtained using the IHR measurement data is in excellent agreement with the ozonesonde data and exhibited a difference of only 5 percent for pressure altitudes between 200 and 60 mb. Above 60 mb the measured ozone profiles diverge. However, the total ozone burden from 200 mb to 10 mb for the two techniques differ only by about 18 percent.

Two initial guess ozone profiles were assumed for the data in Figure 6-2 as starting points for the retrieved IHR profile. The sensitivity of the retrieved profile to the initial guess can be deduced from the width of the line used to show the retrieved profile.

The IHR solar weighting functions which were used to generate the retrieved profile are shown in Figure 6-3 for the three ozone species IF channels. The two lower frequency IF channels (f_c = 370 and 700 MHz) have weighting functions which peak at 10 and 17 km, while the high frequency species (f_c = 930 MHz) channel has a weighting function which peaks at 28 km. It should be noted that the position of the weighting functions were in reverse order to that which would be obtained if there were spectral coincidence between the ozone signature absorption line and the $C^{12}O_2^{16}$ laser LO transition. Therefore, the measurement error at the higher altitudes can be expected to be larger than that at the lower altitudes based on the measured decrease in temperature resolution at the higher IF frequencies in the species channel (refer to paragraph 4.1). The larger deviation between the retrieved and the ozonesonde profile at pressure altitudes above 50 mb (Figure 6-2) can be partially explained by the degradation in the IHR sensitivity at the higher IF frequencies in the species channel.

A second contribution to the divergence between the two measured ozone profiles at altitudes above 50 mb can be attributed to the increase in the relative contribution of atmospheric reemission of the absorbed solar energy in each of the species IF channels. The IF species channel closest to ozone line center (f_c = 930 MHz) is attenuated by all of the intervening atmosphere and, as a result, the IHR measures the lowest effective solar source temperature. The lower effective source temperature results in a

SPECIES CHANNEL	IF CENTER FREQUENCY (MHz)	IF BANDWIDTH
A	370	235
B	700	210
C	930	350
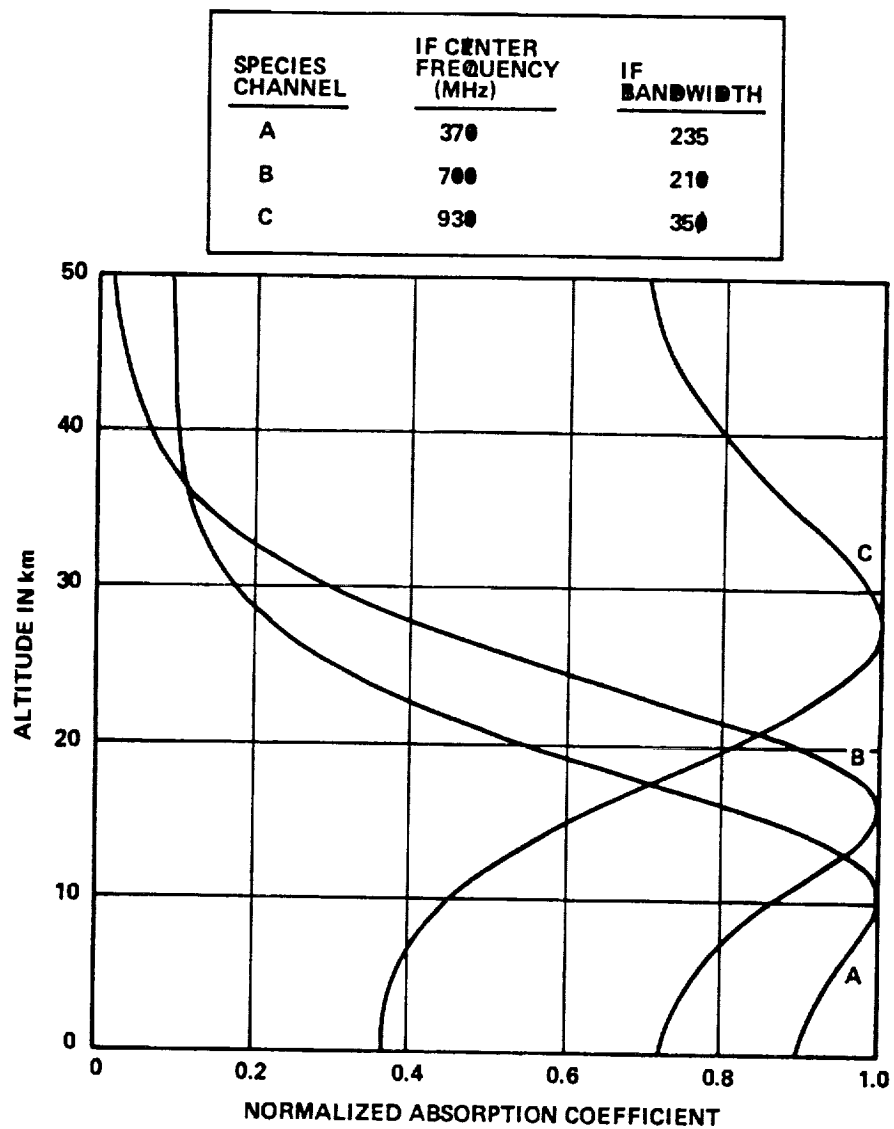
Figure 6-3. Calculated Ozone Weighting Functions for SA Mode (After LaRC)

46

further reduction in IHR temperature resolution at the 930-MHz IF species channel (refer to paragraph 4.1) because of the source temperature dependence on the resolution.

The low elevation solar angle used during the airborne measurements resulted in a relatively long atmospheric path which also decreased the solar radiance at the IHR. The combination of low source temperature due to long path absorption and maximum atmospheric absorption in the 930-MHz IF species channel led to a low apparent source temperature. The atmospheric reemission radiance of the absorbed solar energy has the effect of indicating an artificially higher solar temperature. The corresponding effect on the measurement data is one of reducing the effective measured absorption in the IF channel whose weighting function peaks at 28 km. A lower predicted absorption in this channel results in a retrieved concentration of ozone below that which actually existed in the atmosphere. From Figure 6-2, this can be seen to be the case. The retrieved profile predictably departs from the ozonesonde profile throughout the altitude range covered by the 930-MHz channel weighting function.

For future measurements this effect can be reduced by a more appropriate ozone signature line position and strength. This effect can also be reduced by conducting measurements at higher solar elevation angles. During both the Latitude Survey Mission and the "ASSESS II" Flight Mission, the solar angles were in the range of -3 to +11 degrees to accommodate the requirements of other onboard solar viewing instruments.

6.2 ATMOSPHERIC TRANSMISSION MEASUREMENT FROM 39,000 FEET

A series of measurements were carried out during the Latitude Survey Mission to determine the zenith atmospheric transmission from an aircraft altitude of 39,000 feet. The measurement technique, described in Section 5.0, involves the determination of the received solar radiance as a function of sec θ where θ is the solar zenith angle. The variation of the measured data is equal to the zenith atmospheric attenuation coefficient $\beta(\nu)$ h and the zenith transmission τ_z can be determined using equation 5-8.

For the airborne measurement, the P(20) transition of the $C^{12}O_2^{16}$ laser was used as the local oscillator at a wavelength of $\nu = 1043.1633$ cm^{-1}. The measured solar radiance shown in Figure 6-4 is for elevation angles between $\theta = 4$ and 11 degrees. From this data, the resultant measured atmospheric transmission data indicates that the vertical path atmospheric transmission at the P(20) transition is $\tau_z = 0.89$ above the aircraft altitude of 39,000 feet. As expected, the measured atmospheric transmission from

The graph shows:
- Y-axis: RECEIVED SOLAR ENERGY (ARBITRARY UNITS), ranging from 1 to 6
- X-axis: SECANT θ_S (ZENITH ANGLE), ranging from 0 to 14

Annotations on graph:
VERTICAL PATH
TRANSMISSION ~ 89%

P(24) - $C^{12}O_2^{16}$ LASER
λ = 1043. 1633 cm^{-1}
B = 680 MHz, τ = 3 s, FL 14
PRESSURE ALTITUDE $\approx$ 39,000 FEET
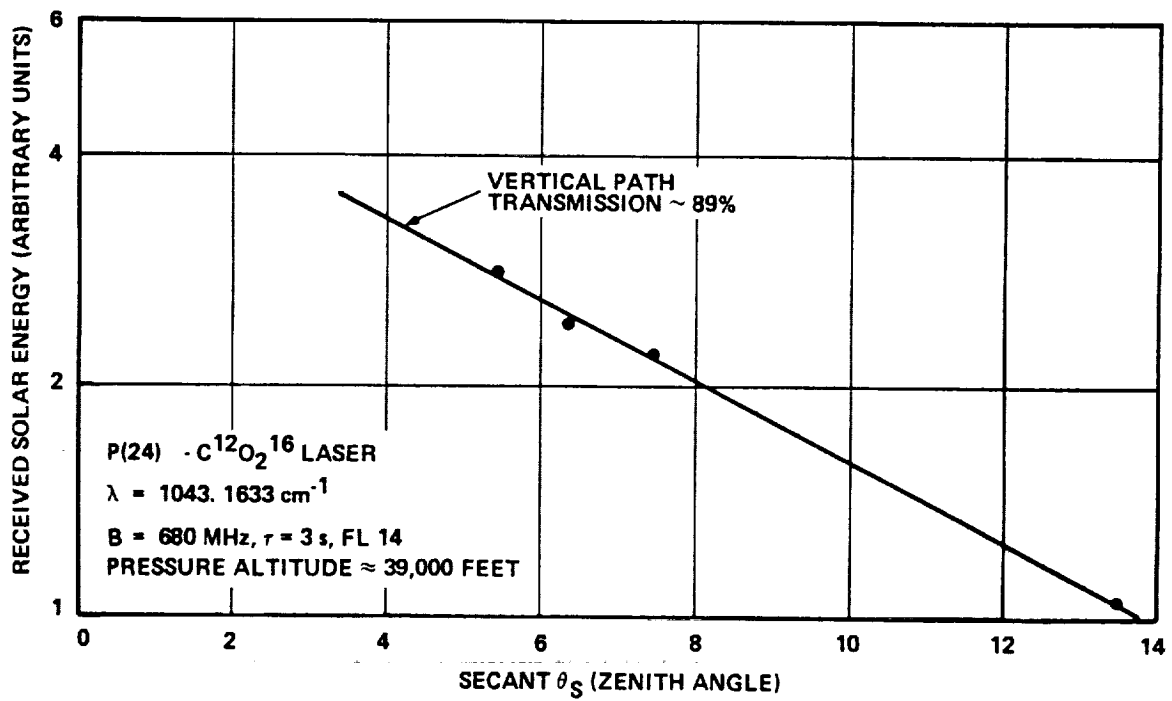
Figure 6-4. Variation of Solar Radiance Collected at IHR Versus Secant of Solar Angle

48

the airborne platform is considerably higher than the τ_z = 0.41 to 0.59 values measured with ground-based IHR's.

6.3 NADIR RADIANCE MEASUREMENTS

Some initial nadir radiance measurements were carried out during the Latitude Survey Mission. During this mission most of the flight paths were over water and very little time was available over urban centers where substantial tropospheric ozone concentrations could be expected. Using the Dicke measurement mode, a series of nadir measurements were carried out over northern Alaska to determine how well the IHR reference channel tracks the actual ground temperature (provided by the onboard NOAA surface temperature broadband radiometer). The results shown in Figure 6-5 for a ground temperature variation of 20°C, indicate that the IHR reference channel appears to track the ground temperature over the 3-minute measurement period. From this data it appears that the reference channel will be effective in minimizing the effects of changes in ground brightness temperature when the IHR is operated in the NR mode.

On the following ASSESS II flight program, the local oscillator optics were redesigned to increase the temperature resolution of the species photomixer. With the increased temperature resolution some species channel data was obtained in the nadir radiance mode. A 1-hour sample of this data is shown in Figure 6-6. The measurement interval chosen for data reduction begins at 12:26 and concludes at 12:46.

The selected data includes a hot black body calibration segment (T_c = 333 K), an ambient black body segment (T_c = 293 K) and a nadir ground temperature measurement.

The IHR voltage outputs are plotted in Figure 6-7 in order to determine the apparent nadir temperature and therefore the upwelling irradiance of the earth and the intervening atmosphere. The two known radiances (for T_c = 293 and 333 K) and their respective output voltages provide a calibration of output voltage per source radiance in each of the IHR channels. The ground (plus atmospheric) radiance is obtained by locating the nadir measurement voltage on the line joining the two calibration data points and then directly reading off the source radiance. There is no need to take the individual channel bandwidths into account because they only affect the radiometer signal to noise (SNR) and not the apparent source temperature.
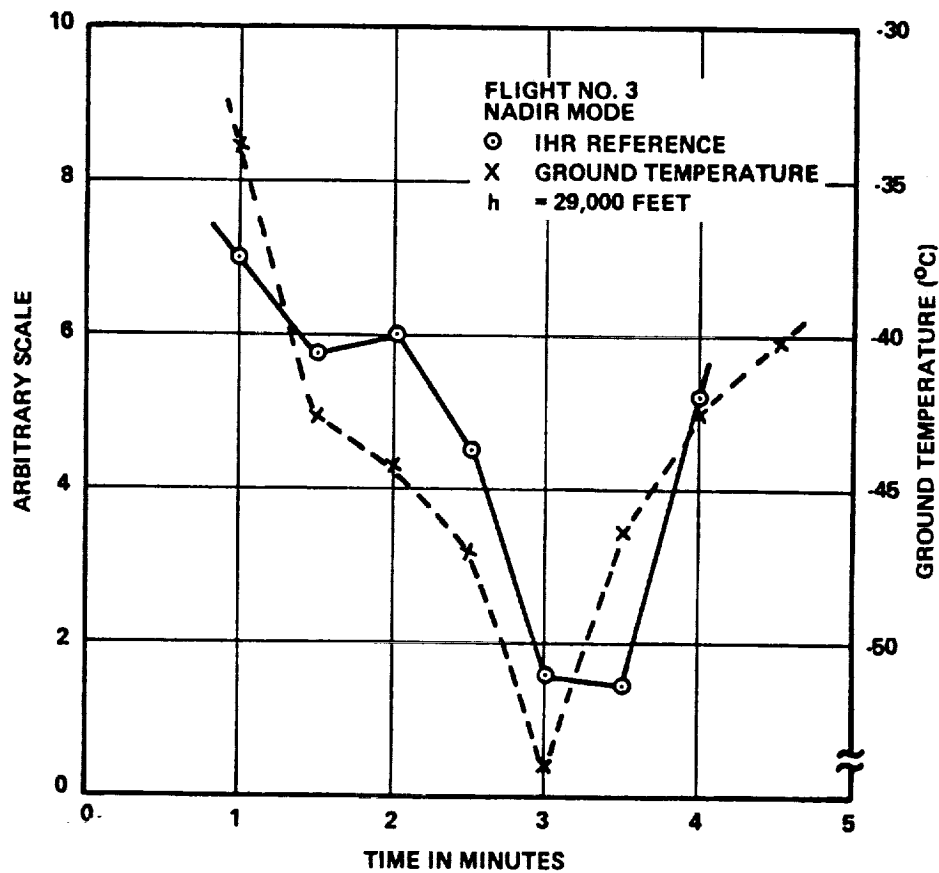
Figure 6-5. Measured Variation of IHR Reference Channel and Ground Temperature Versus Time in Nadir Radiance Mode

50
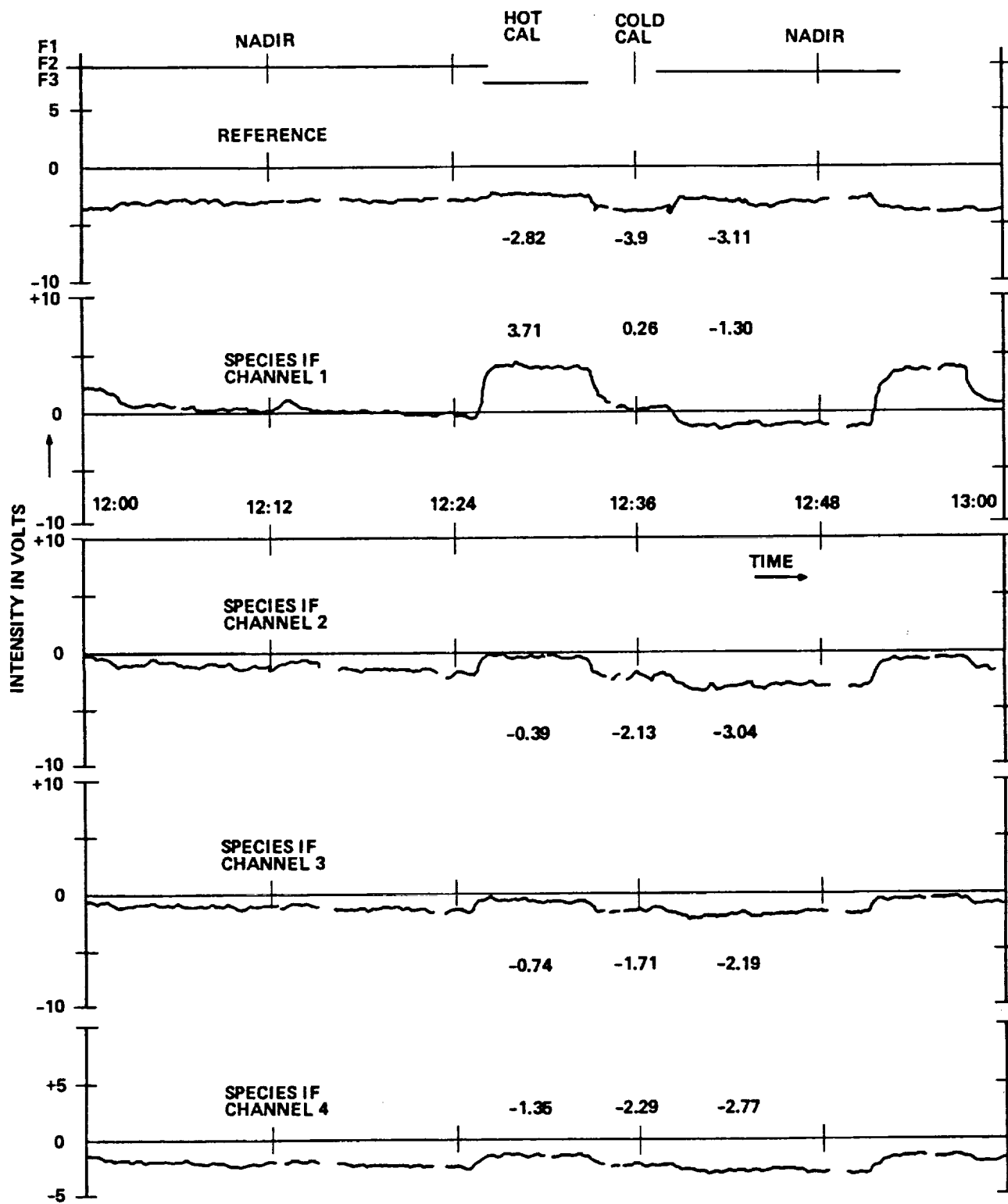
Figure 6-6. IHR Nadir Radiance Measurement Data Collected on CV-990 Flight Test (τ = 10 Seconds)
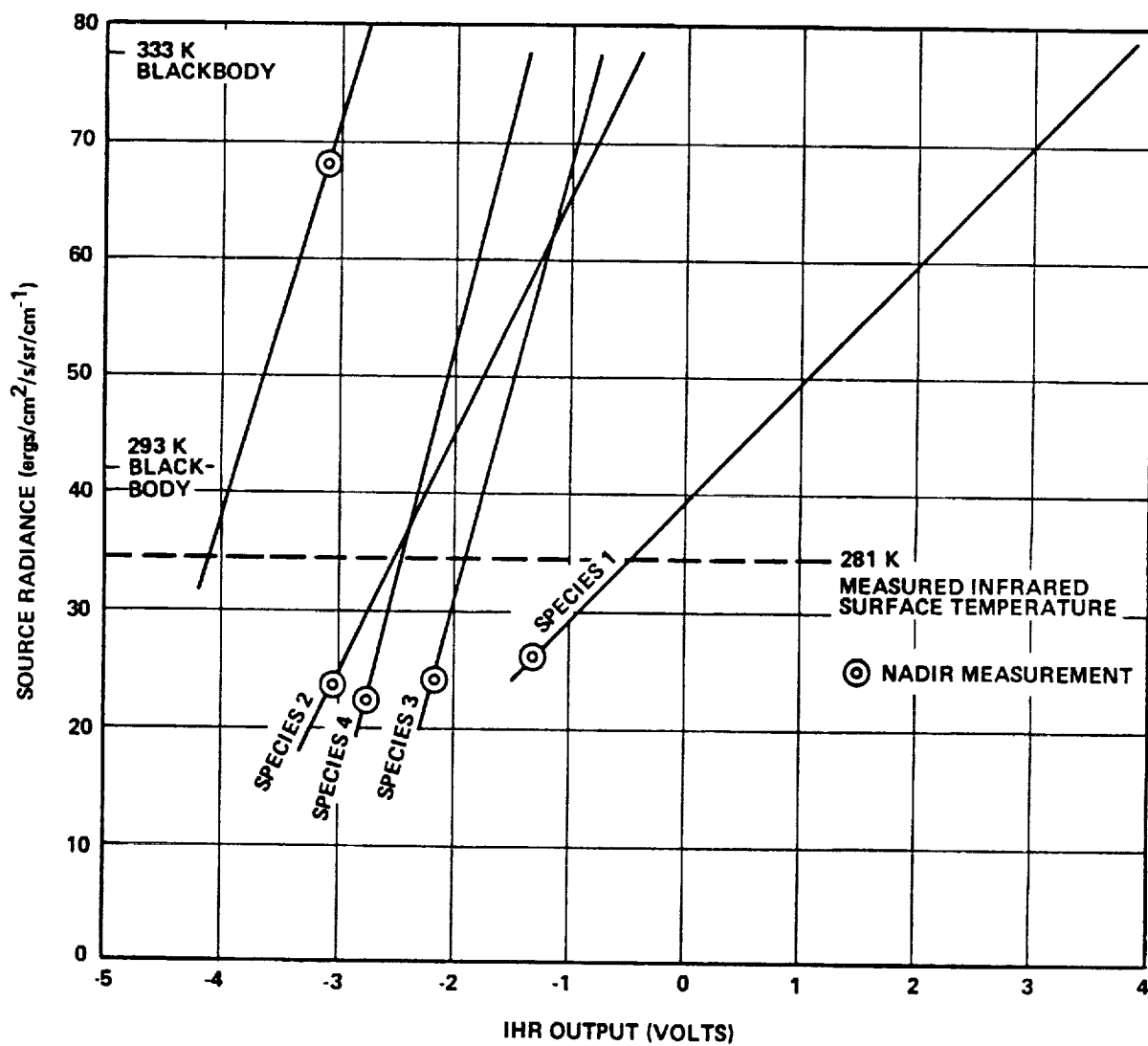
Figure 6-7. IHR Nadir Radiance Measurements Using P(14) and P(24)
Transitions of $C^{12}O_2^{16}$ Laser

Upon inspection of the measured data in Figure 6-7, it can be seen that the IHR reference channel indicates a source radiance of 68 ergs/cm^2/sec/sr/cm^{-1} which corresponds to an equivalent temperature of $T \approx +50^{\circ}C$, while the species channels indicated a source radiance of approximately 24 ergs/cm^2/sec/sr/cm^{-1} ($T \approx -7^{\circ}C$. These temperatures can then be compared to the broadband (8 to 12 μm) NOAA infrared surface temperature radiometer which indicated a relatively constant temperature of $+8^{\circ}C$. The values for the species channel appear to be within reason. However, the reference channel contains a $42^{\circ}C$ temperature error which is believed to be due to laser LO retroreflections in the IHR (refer to Appendix A, paragraph A.1.7). Since the LO retroreflection can vary with optical path and time, its net effect cannot be removed from the data to allow direct data reduction. A small offset due to LO retroreflections may also be present in the species channel.

The results of the initial nadir radiance measurements demonstrate the potential of obtaining tropospheric ozone data in the Dicke mode using the upwelling radiance of the earth and the atmosphere. Instrument difficulties involving the retroreflection of LO power are presently limiting the ability of the IHR to obtain an ozone burden in the NR measurement mode. Techniques are presently available to eliminate the retroreflections. However, they involve a new layout of the optical train. Insufficient time was available during the AAFE program of the ASSESS II Mission to implement these modifications.

The presently available IHR temperature resolution will be the eventual limitation in obtaining remote tropospheric species profiles using the earth as the back-lighting source. Some improvements can be made in the areas of heterodyne efficiency and reducing optical losses. However, the major improvements are expected to be in the photomixer quantum efficiency and optimum photomixer amplifier interface design. In addition, effective reference channel tracking and improved IHR stability may allow IHR integration times which approach 1 minute, or more.

53

7.0 CONCLUSIONS

This instrument development and flight-test program has success-fully demonstrated the use of a new radiometric instrument, the Infrared Heterodyne Radiometer, for remotely detecting, monitoring, and tracking the concentration, vertical distribution, and spatial extent of natural and man-made atmospheric molecular constituents having vibrational-rotational spectral lines which overlap available infrared laser local oscillators.

Some specific advantages of the IHR sensor over other presently available remote sensors include:

- High specificity for unambiguous monitoring

- High sensitivity approaching quantum-noise-limited operation

- Diffraction limited field-of-view which results in a relatively small spatial footprint

- A completely passive sensor which does not require a high power laser transmitter

- Use of a clear spectral channel to improve the overall measurement accuracy

Ground-based IHR measurements of atmospheric ammonia ($\lambda \approx 10.8\ \mu m$) and ozone ($\lambda \approx 9.6\ \mu m$) have been carried out in the solar absorption (SA) measurement mode. Although no ground truth data was available during these measurements, the ammonia and ozone profiles yielded values which were within the range of previously measured values.

Airborne SA measurements, carried out on the NASA CV-990 test aircraft, resulted in atmospheric ozone profiles at several latitudes. These profiles exhibited latitude variations of the peak ozone concentration which were in good agreement with the expected values, although no ground truth data was available to corroborate these measurement results. Remote SA airborne measurements during the ASSESS II (simulated space shuttle) Mission resulted in atmospheric profiles which were in excellent agreement with coordinated in situ and ozonesonde measurement data.

Airborne measurements have also been initiated in the nadir radiance (NR) mode. Preliminary data indicates tracking between the IHR reference channel and an onboard broadband ground temperature radiometer. Additional IHR modifications are required before NR measurements of tropospheric species profiles can be carried out. The capability for rapid switching between laser local oscillator transitions permitted operation in several modes (that is, SA, NR, and atmospheric propagation) at several spectral locations during a single test flight.

Other atmospheric species with vibrational-rotational spectral lines in the 9 to 11 μm region which may be candidates for remote profiling with the existing dual channel IHR include HNO_3, ClO, NO_2, Freons, and HCl. In addition, IHR's have been developed in the 2 to 5 μm spectral region for atmospheric propagation measurements at the HF, DF, and CO laser wavelengths.[30,31]

Ongoing efforts aimed at developing cooled tunable-diode lasers (TDL's) which can be used as local oscillators in the IHR's are expected to extend the measurement capabilities of this instrument to a large number of gas species with isolated infrared absorption spectra. The TDL's can be designed to operate in selected portions of the 3 to 30 μm spectral region. The tunability of the TDL's may permit precise atmospheric profiling using only two relatively narrowband IF channels.

Recent investigations indicate that the IHR can also be used to remotely determine the vertical temperature profile of the atmosphere using CO_2 vibrational-rotational spectral lines near $\lambda = 13.25$ μm.[32,33]

Regional atmospheric profiling measurements have been shown to be valid from airborne platforms. Future application of this instrument should include global monitoring of atmospheric species from satellite platforms such as the space shuttle.

APPENDIX A
IHR SYSTEM DESCRIPTION

A.1 OPTICAL PACKAGE

The IHR optical package top and bottom views are shown in Figures A-1 and A-2, respectively. The design of this package is based on a lightweight, stiff aluminum honeycomb plate (1-1/2 inches thick) to which all of the optical components are attached. The skins of the honeycomb have been made sufficiently thick so that all components can be directly mounted using tapped holes in the skin. This approach permitted maximum flexibility in the optical design. The edges of the honeycomb plate have been reinforced with aluminum bar stock to facilitate mounting. In addition to the epoxy bonding of the honeycomb, skin, and bars, the assembly has been through-bolted around the perimeter in order to meet the crash safety standards[A-1] of the NASA CV-990 test aircraft. Mounting brackets for use in the aircraft are attached to the side of the honeycomb plate and secured through the honeycomb skin and the aluminum bar stock. Vertical side plates were attached to the honeycomb baseplate in order to support the dust covers and provide an attachment point for all the bulkhead electrical, vacuum, and water connections.

A.1.1 CO_2 Laser LO Mounting

The bottom view of the optical package (Figure A-2) shows two commercially available (Honeywell 7000) CO_2 lasers rigidly mounted to the honeycomb plate. Two 45-degree mirrors are used to reflect the CO_2 laser beams to the top side of the honeycomb plate. Also shown mounted on the bottom of the honeycomb plate are the bias circuits for the photomixers, together with adjustment pots for setting the optimum photomixer bias voltage.

Each of the CO_2 lasers has a set of ballast resistors mounted on the side of the laser. The ballast resistors and CO_2 laser tubes are water cooled. A flow switch has been provided in the cooling circuit to shut off the laser power supply and prevent damage to the laser in the event of a water cooler malfunction. The grating wavelength adjustment micrometers can be seen projecting through the side walls of the package for readily accessible adjustment of the laser wavelength.
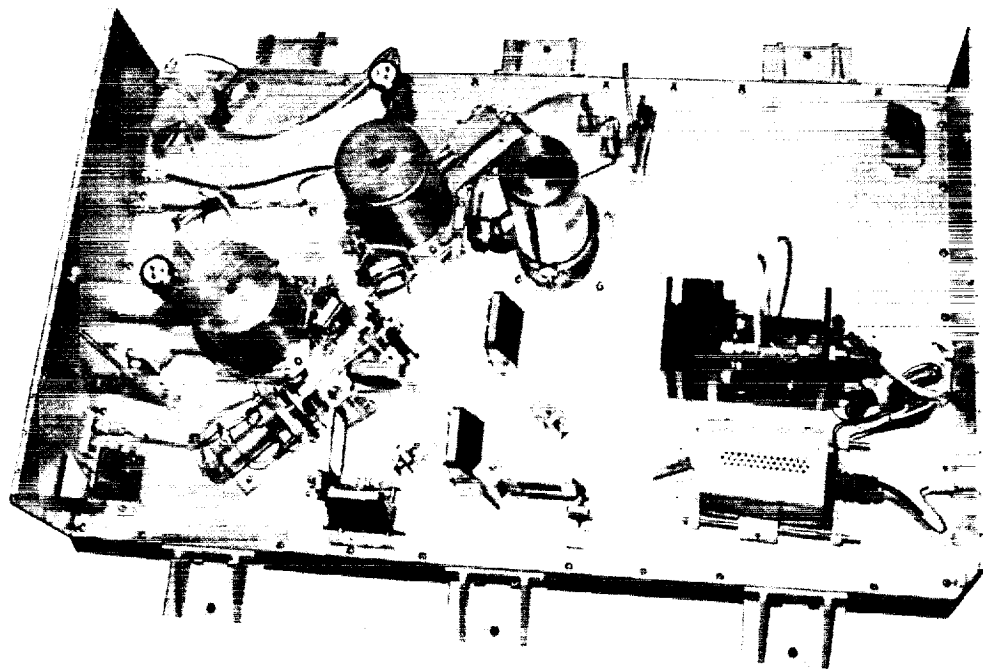
Figure A-1. Optical Package - Top View

58
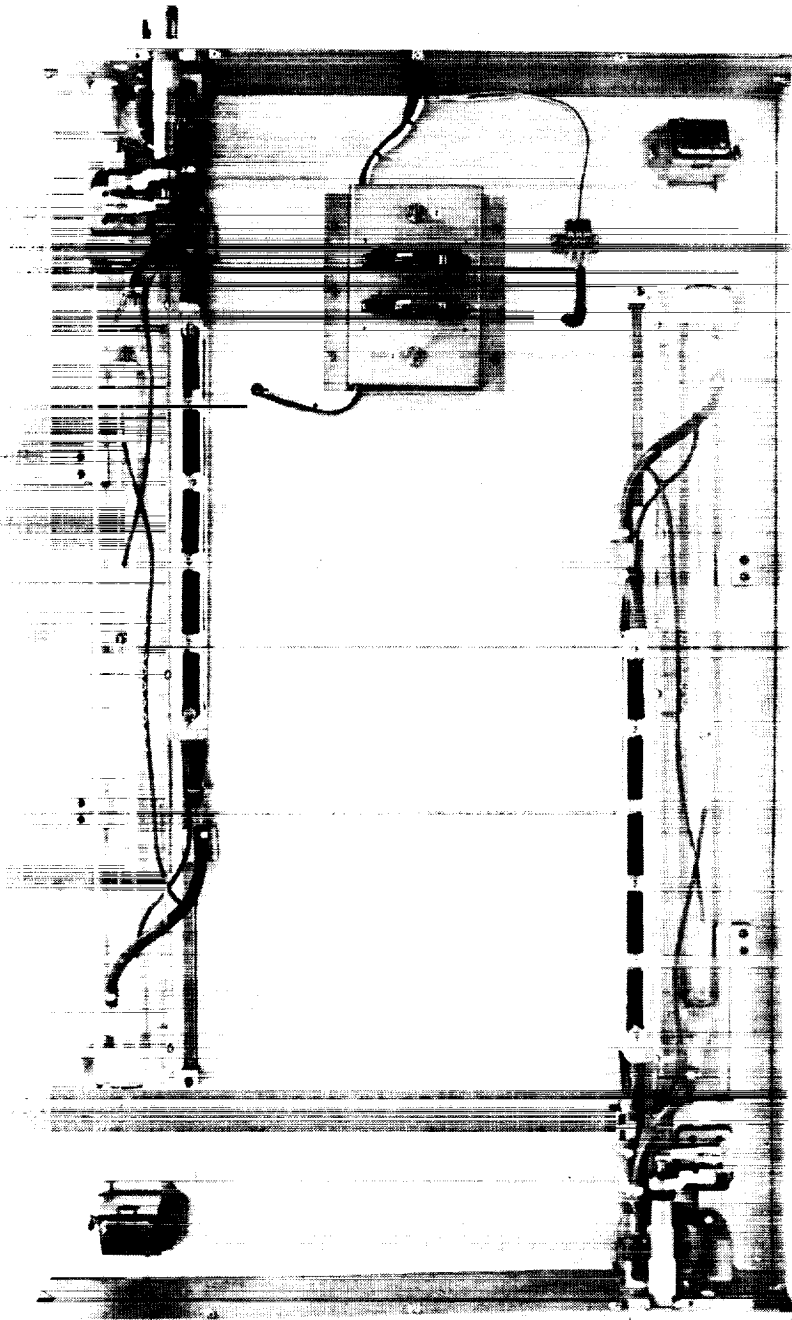
Figure A-2. Optical Package – Bottom View

59

The adjustment mechanism as well as the laser cavity structure was modified from the original commercial laser design prior to the aircraft flight testing. The commercial unit was found to be highly susceptible to vibration which limited the temperature sensitivity of the IHR. As a result, the laser cavity structure was modified from an L-shaped channel to an elongated U-shaped yoke structure with an integral bottom plate. This ruggedized laser unit, together with an improved grating mount, effectively reduced the laser vibration susceptibility.

Bulkhead connectors were provided on the sides of the optical package in order to supply the high voltage to the laser heads from the external high voltage power supplies. Due to the split discharge design of the laser, two power supplies are employed for each laser head.

A.1.2 Collecting Telescope

An optical diagram of the top surface of the optical package (Figure A-1) is shown in Figure A-3. The scene radiance is collected using a 2-inch diameter (f/6.5) germanium collecting lens. This lens focuses the incoming radiance onto the two PV:HgCdTe photomixers whose sensitive areas are matched in order to assure that the two radiometer channels have approximately the same field-of-view (FOV).

A.1.3 Optical Band-Pass Filter

Before reaching the Dicke-switch, the incoming radiance is optically filtered by an 8-μm long-pass filter. This filter is used to limit the amount of solar radiance which reaches the photomixers. Since the peak of the solar radiance occurs in the near infrared, a large portion of the superfluous solar radiance is blocked by this filter.

A.1.4 Optical Dicke-Switch

A rotating optical disc located in the path between the input lens and the photomixers acts as the Dicke-switch. The disc is positioned at an angle of 45 degrees with respect to the incoming focused scene radiance and was designed to alternately pass and reflect the scene radiance. The 3-inch diameter disc is made of zinc selenide (ZnSe). Its front surface is one-half antireflection coated (less than 1 percent reflection) and the other half of the disc front surface is high reflectivity coated (greater than 98 percent). The second (rear) surface is fully antireflection coated. The alternate high and low reflectivity coatings on the front surface reflect or transmit the incoming radiance to the two photomixers as the disc is rotated.

60
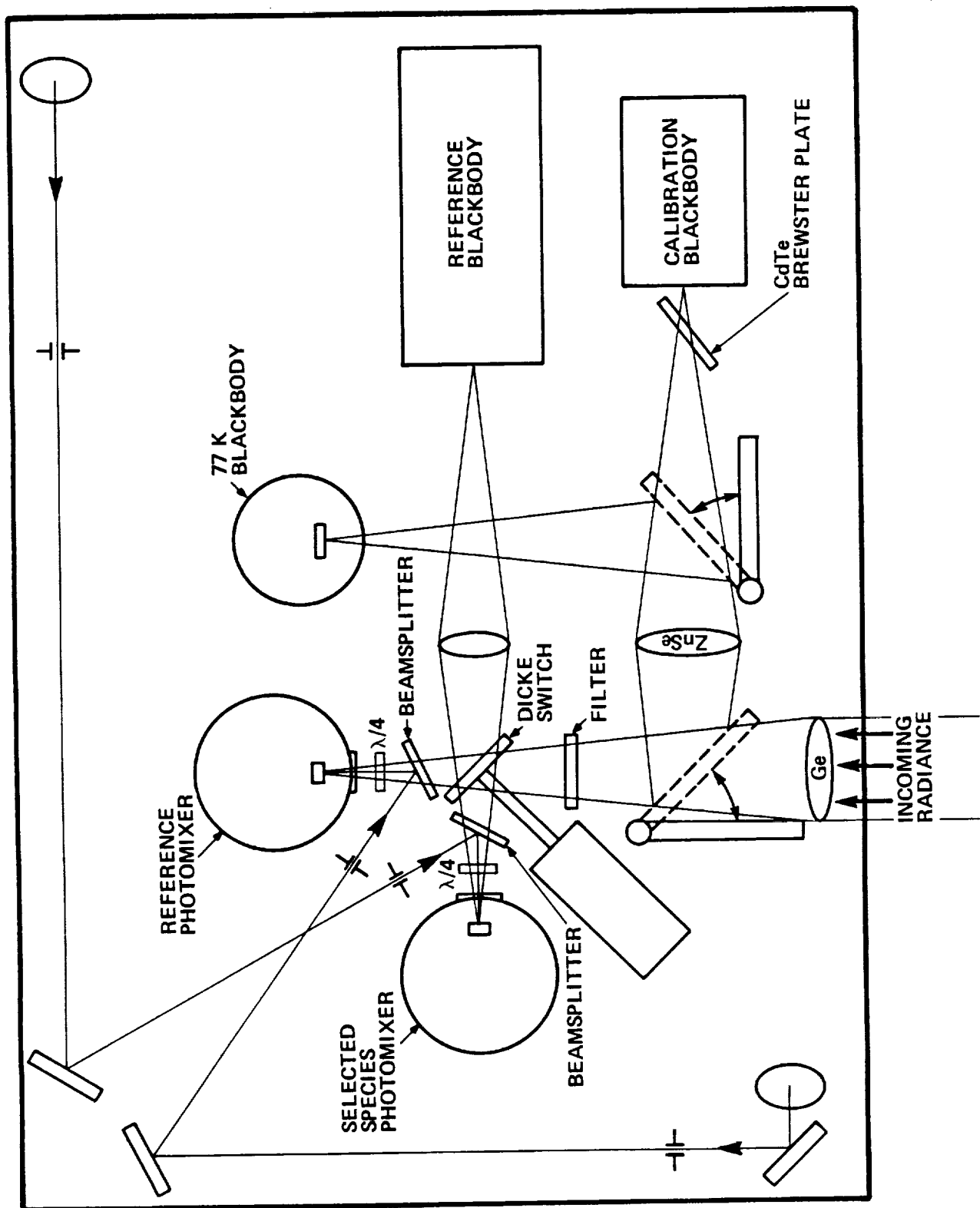
Figure A-3. Simplified Optical Diagram of Top Surface of IHR Optical Package

The Dicke-switch is rotated by means of a brushless dc motor whose speed is variable between 600 and 6000 rpm. Since one rotation of the Dicke-switch corresponds to one chopping cycle, the Dicke chopping frequency is adjustable from 10 to 100 Hz. The adjustable chopping frequency gives the flexibility of operating the IHR at frequencies which are offset from any structural resonances found in the IHR or the aircraft. Mounted on the shaft joining the motor and the Dicke-switch is a second disc which provides a sync signal for the electrical processors. The sync pulse is derived from the rotation of an iron post (mounted on the disc), past a magnetic transducer which generates a current impulse. Two transducers are used to eliminate the 180-degree phase ambiguity for the photomixers which view the scene on alternate half cycles of the Dicke-switch.

When the Dicke-switch is positioned such that a particular photomixer is not exposed to the scene radiance, it views a temperature controlled black body that provides a reference temperature for comparison with the scene or calibration source radiance. Both photomixers view this reference black body on alternate half cycles to provide a radiance comparison between the two infrared radiometer channels. The reference black body is set to approximately match the scene radiance in the NR mode, and is set to ambient temperature for the SA mode.

A.1.5 Black Body Calibration

A flip mirror is provided for insertion of a calibration black body into the path between the input lens and the Dicke-switch. This calibration black body is viewed by the photomixers through a ZnSe lens in order to have the black body source fill the field of view of the photomixer. The temperature of this calibration black body can be varied from 325 to 1300 K with the calibration temperature being chosen to be slightly higher than the scene temperature whenever possible. A second flip mirror is located behind the ZnSe lens to provide a calibration temperature (77 K liquid nitrogen dewar) which is lower than the scene temperature. Two calibration temperatures are required to: (1) determine the temperature/voltage responsivity of each IF channel processor and (2) permit comparison between the source radiance IF channels and, therefore, fix the spectral characteristics of the integrated atmospheric absorption.

The temperature controllers for both the reference and high temperature black bodies are rack mounted and located external to the optical package. A separate bulkhead connector is provided on the side wall of the optical package for supply and control of power to each black body.

A.1.6 LO Injection

A beam splitter is located between the Dicke-switch and the photo-mixers to inject local oscillator power into the optical path of each photomixer. The beam splitter has a 10 percent reflection coating on the surface adjacent to the photomixer and an antireflection coating on the opposite side. The beam splitter, therefore, transmits 90 percent of the scene (or black body) radiance to the photomixer and reflects 10 percent of the available LO power onto the photomixer. This method of LO injection provides the benefit of a low loss of the signal radiance together with an attenuation of the powerful CO_2 laser output. Each PV:HgCdTe photomixer requires approximately 1 milliwatt of LO power, while each laser output is on the order of 1 watt.

A front surface gold mirror mounted at 45 degrees to the honeycomb plate reflects the LO power from the underside of the baseplate parallel to the plane of the baseplate at a height of 2 inches. A second mirror was necessary in the reference LO path in order to properly reorient the LO polarization with that of the pollutant LO. In each path following these mirrors, the LO beam passes through an adjustable iris which serves as a fine control on the LO power incident on the photomixer.

Between the adjustable iris and the photomixer, a solenoid operated LO beam blocking flag was inserted which was controlled by the photomixer bias circuit. This was provided as a safety measure to prevent excessive amounts of LO power from accidentally damaging the photomixer. As the LO power is increased, additional photoinduced current is generated in the photomixer and when this current reaches a preset level of approximately 2.0 mA, the bias circuit trips out and releases the flag to block the LO beam.

A.1.7 LO Isolator

An optical isolator was found to be necessary in order to reduce the LO reflection from the photomixer and its mount. LO power which is not absorbed by the photomixer and its mount is reflected back through the beam splitter into the IHR optical train. This reflected power passes through the optical Dicke-switch and a portion of it is reflected by each component of the optical train. This reflected power passes back through the Dicke-switch and is incident upon the photomixer. These retroreflections can be very efficient in the case of the input lens due to the concave shape which efficiently focuses the retroreflections back onto the photomixer. It is also very efficient for reflections from the calibration black body due to the relay lens which focuses the diverging LO power onto the black body. All retroreflections are then efficiently controlled by the relay lens and imaged back onto the photomixer.

63

These retroreflections of LO power would be of little consequence to the IHR if they were not interrupted by the Dicke-switch at its chopping rate. The minor amount of shot noise generated in the photomixer due to this reflected LO power has little or no effect on the heterodyne sensitivity, when compared to the 1-mW LO power level in the photomixer. However, when it is modulated at the Dicke-switch frequency, the synchronous detection of the IHR senses it as a signal which adds or subtracts from the black body temperature being measured. Since these reflections are not controlled, they can vary randomly due to component vibration and temperature change of the instrument. As a result of these random vibrations in reflected radiation, the IHR output has a random vibration which can make accurate low level measurements very difficult.

The optical isolator used in the IHR during the Latitude Survey Mission was a quarter-wave plate located between the LO beam splitter and the photomixer. Linearly polarized LO power passes through the $\lambda/4$ plate and is changed to circular polarization. Upon reflection from the photomixer and its surroundings, the direction of rotation of the circular polarization is reversed. When this reflected LO power passes back through the $\lambda/4$ plate it is converted back to linear polarization; however, its polarization angle has been rotated by 90 degrees. Since polarized reflection from surfaces which are not normal to the beam can be significantly different for orthogonal polarizations, some degree of isolation (reflection out of the normal optical path) is achieved at each optical surface encountered. Examples of these surfaces are: (1) LO beam splitter, (2) Dicke-switch, and (3) cadmium telluride plates which have been placed in front of the black bodies at Brewster's angle (angle for optimum isolation and minimum signal attenuation). The maximum isolation can then be obtained using this technique and will be approximately 100:1.

The aircraft vibration encountered on the Latitude Survey Mission accentuated the variation of retroreflected LO power limiting the usable flight data in the NR (downward viewing) mode.

The LO retroreflected signal can further be reduced by limiting the amount of LO power incident upon the photomixer. The inclusion of a beam expander and a focusing lens for use with the focused LO spot matched to the photomixer area will limit the retroreflected power to less than 0.1 milliwatt. It is believed that the laser LO power reduction together with a judicious cocking of the photomixer mount and a slightly revised optical design will completely eliminate the retroreflection effects in the existing IHR.

A.1.8 Photomixers

The two PV:HgCdTe photomixers are mounted in liquid nitrogen dewars. The dewars have been modified for aircraft use by the addition

of direct structural supports for the cold plate. This modification was intended to prevent misalignment of the photomixer position with respect to the infrared source and laser LO paths that may be caused by vibration or tilting of the optical package.

The IF output of the reference photomixer passes through a connector on the wall of the dewar to an IF preamplifier which provides 30 dB of gain. The atmospheric species (pollutant) photomixer dewar includes a specially designed wideband IF amplifier which is mounted in close proximity to the photomixer. This cooled preamplifier provides greater system sensitivity in addition to eliminating any frequency dependent impedance mismatch effects which may be caused by 50-ohm coaxial cable between the photomixer and amplifier. The internal IF amplifier provides approximately 10 dB of gain. The output of this preamplifier is coupled through a hermetically sealed connector on the dewar wall to a second IF amplifier which provides an additional 26 dB of gain. The outputs of the two IF amplifiers are then fed by low loss coaxial cable to the electronic processors.

A.2 BIAS CONTROL PANEL

The bias control unit shown in Figure A-4 (third from the top in right-hand bay) is a separate rack-mounted chassis which supplies dc power to the optical package, controls the Dicke-switch motor, controls the photomixer bias, and provides a monitor for the photomixer bias voltage and current on a digital display. This package also takes the sync pulses from the Dicke-switch in the optical package and processes them to provide a square-wave sync signal for switching the processors. It should be noted that the reference and species synchronous processors are 180 degrees out of phase. Table A-1 lists the various controls and indicators for the bias control panel.

A.3 WATER COOLER FOR LASER

A Neslab closed cycle water cooler is provided for control of the water temperature in the laser heads. The cooler unit is remotely mounted from the optical package and operates on 115 Vac. It can provide ±0.1 K temperature stability from -20 to +30°C. The lower temperatures are required when operating the laser LO's on the low gain transitions. The interior structure and the casing of the refrigerator unit were substantially strengthened to meet the crash safety requirements of the CV-990 test aircraft.

A.4 RADIOMETER SIGNAL PROCESSOR

The IHR signal processing back-end consists of four rack-mounted units. The first processor, which has a bandwidth of 680 MHz, is employed as the reference channel. The remaining three units process information in
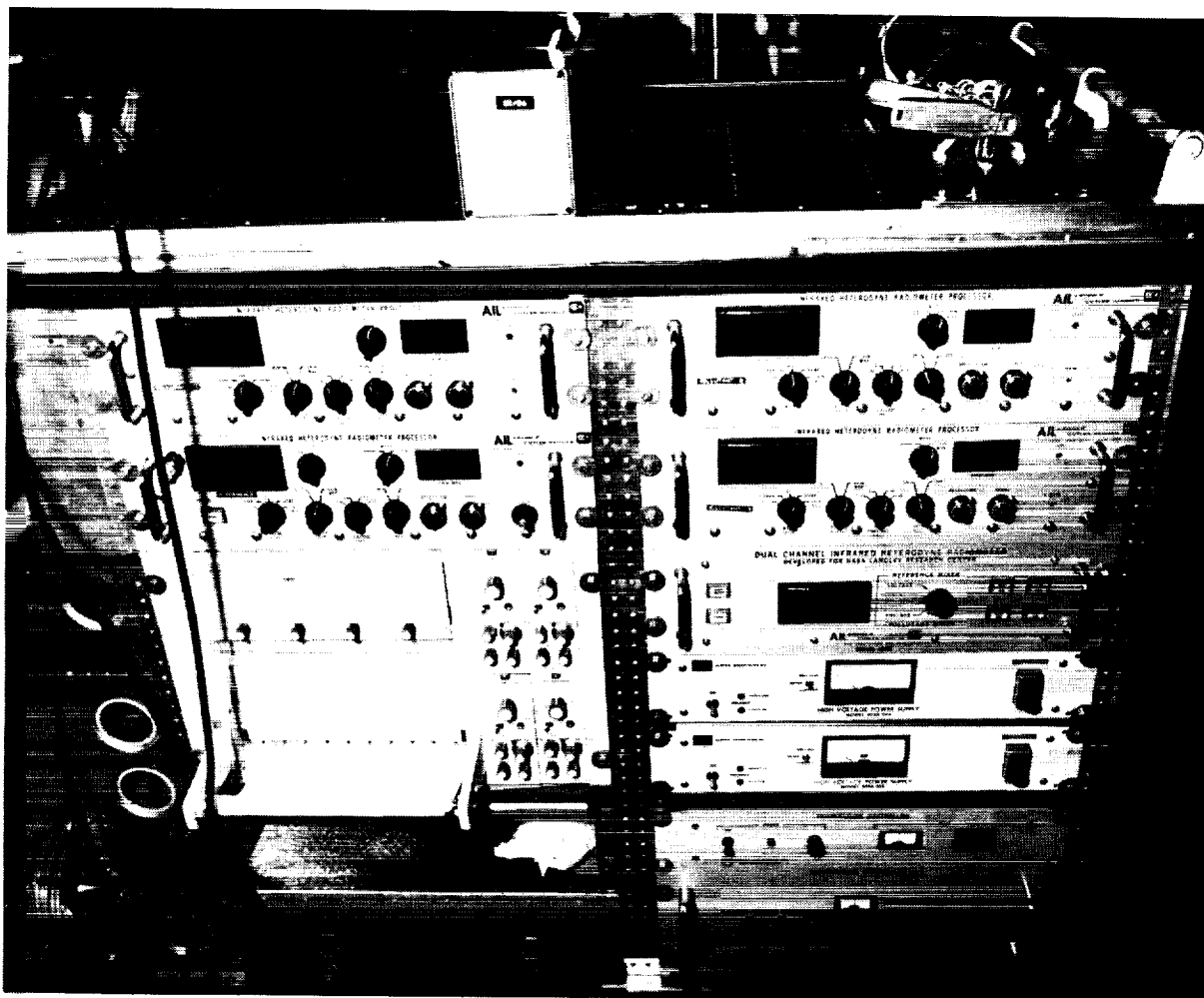
Figure A-4. IHR Control and Processing Electronics Mounted Aboard CV-990

66

Table A-1. Controls and Indicators for Bias Control Panel

Control or Indicator	Function
POWER	Supplies power to bias control panel.
DICKE-SWITCH	Activates Dicke-switch motor.
REFERENCE MIXER BIAS	Supplies power to reference IF amplifier and bias control circuit.
RESET REFERENCE BIAS	Applies bias to photomixer which latches relay if current within range.
POLLUTANT MIXER BIAS	Supplies power to pollutant IF amplifier and bias control circuit.
RESET POLLUTANT BIAS	Applies bias to photomixer which latches relay if current within range.
REFERENCE MIXER { VOLTAGE CURRENT	Monitors reference photomixer bias voltage or current.
POLLUTANT MIXER { VOLTAGE CURRENT	Monitors pollutant photomixer bias voltage or current.

the species channel. The reference channel processor unit also contains dc power supplies, IF power splitters, and the circuitry which provides the synchronizing signals for the four radiometer signal processing channels and the data management system. The three species channels each had a 500-MHz bandwidth and operated over the following frequency ranges for the Latitude Survey Mission:

Species Channel No. 1   150-650 MHz

Species Channel No. 2   650-1150 MHz

Species Channel No. 3   1150-1650 or 1650-2150 MHz

A.4.1 Operational Modes for IHR Processors

The signal processors have the capability of operating in the Dicke-switched or self-balancing gain modulation mode. The IHR input is rapidly switched between the unknown source temperature and a constant temperature reference black body.

The Dicke-switched mode provides a conventional temperature comparison measurement for the IHR. The ac switch rate component from the IF detector, which represents the temperature difference between the compared sources, is ac amplified and synchronously detected to provide a voltage which is proportional to the temperature difference. This voltage, after selectable low-pass filtering, is available for recording and is displayed on a front panel meter.

In the Dicke mode, the radiometer signal processor output (V_o) can be expressed in the form:$^{A-2}$

$$V_o = G_S (T_A + T_e) - G_R (T_R + T_e) \qquad \text{(A-1)}$$

where:

T_A = unknown source temperature

T_R = reference temperature

T_e = effective temperature of the electronics

G = overall gain

G_S = radiometer gain when the photomixer is viewing the unknown source

G_R = radiometer gain when the photomixer is viewing the reference

and when $G_S = G_R = G$, then:

$$V_o = (T_A - T_R)\, G$$

When the Dicke radiometer is at null balance, the unknown source temperature T_A is equal to the reference temperature T_R. For this case, system gain variations will be eliminated and the effects of gain instabilities from the LO lasers through the processors will be eliminated.

If the radiometer is not at null balance, a differential error (ΔV_o) can occur in the event of system gain variations, ΔG. This can be expressed:

$$\Delta V_o = (T_A - T_R)\, \Delta G \tag{A-2}$$

When the IHR is operated in the nadir radiance (NR) mode, it becomes important to set the temperature of the reference black body close to the "apparent" temperature of the unknown source to reduce the effect of IHR gain instabilities. This temperature matching can easily be accomplished over the small range of temperatures encountered when viewing the earth.

However, when the IHR is operated in the solar absorption (SA) mode, a very large range of temperatures are encountered which can generate significant error voltages due to system gain variations. Gain modulation was chosen as the processing technique to reduce these gain instability errors.[A-3]

The gain modulation method varies the radiometer gain in synchronism with the Dicke-switch. The IHR stability is improved by varying the gain, G_R, such that $V_o = 0$. Sensitivity to gain variations can be reintroduced, however, if the source temperature, T_A, changes after the gain, G_R, has been set. Since the output voltage will no longer be zero, the gain instabilities will, again, be apparent.

In the self-balancing gain modulation mode used in these signal processors, a non-zero output of the gain modulated radiometer is detected and balance is maintained by providing adaptive gain control. The mechanism by

which gain control is effected can be either active (gain should be >1) or passive (gain is ≤1). Since passive controllers have the inherent advantage of being more stable, this type of control is employed in discrete steps (digital). The use of digital attenuators simplifies the interface to the data recording equipment and offers the advantages of the inherent accuracy of digital video frequency attenuators. Figure A-5 shows a simplified block diagram of a self-balancing gain modulation signal processor.

Source irradiance and reference irradiance are alternately switched by the Dicke-switch to the coherent detection subsystem which detects the infrared energy and translates it to an IF frequency. The IF signal is then detected and dc amplified. Separate circuitry, which is synchronized to the Dicke-switching frequency, is used to control the lower limit of the temperature measurements and resolution of the output in counts per degree (Figure A-6). The output of the signal processor amplifiers is synchronously detected and integrated by means of an RC low-pass filter which limits the measurement noise and sets the system time constant. The difference (error) between the unknown source and reference source is then used to vary the gain during the reference cycle of the Dicke-switch and drive the error sensor to zero. A binary attenuator is used in the feedback to the reference gain control in order to provide a digital output of the source temperature. The level of the binary attenuation is, therefore, directly proportional to the unknown source irradiance. The data output is then converted from binary to BCD which can be read out on the LED display on the front panel, or recorded by the Data Management Subsystem. The attenuator is a 10-bit binary and it may assume values between 0 and 1023/1024 in steps of 1/1024.

The self-balancing gain modulation method thereby maintains the output at null and prevents errors due to IHR gain instabilities. The method also has the significant advantage of providing a long time constant, τ, during steady state conditions and a much shortened effective time constant when following a transient in source temperature. This provides a significant advantage for the solar occultation mode which is expected to be used during the space shuttle measurements. Since the shuttle measurement time will be short (~30 to 60 seconds), a processor with this adaptive time constant will be better able to handle the large transient in source temperature associated with solar acquisition, and any other transient phenomena associated with scanning the various atmospheric layers.

A.4.2 Radiometer Signal Processor Operating Controls

The controls and indicators described in Tables A-2 and A-3 are shown in Figures A-7 and A-8 and pertain to the operation of the reference and pollutant channel signal processors as noted.
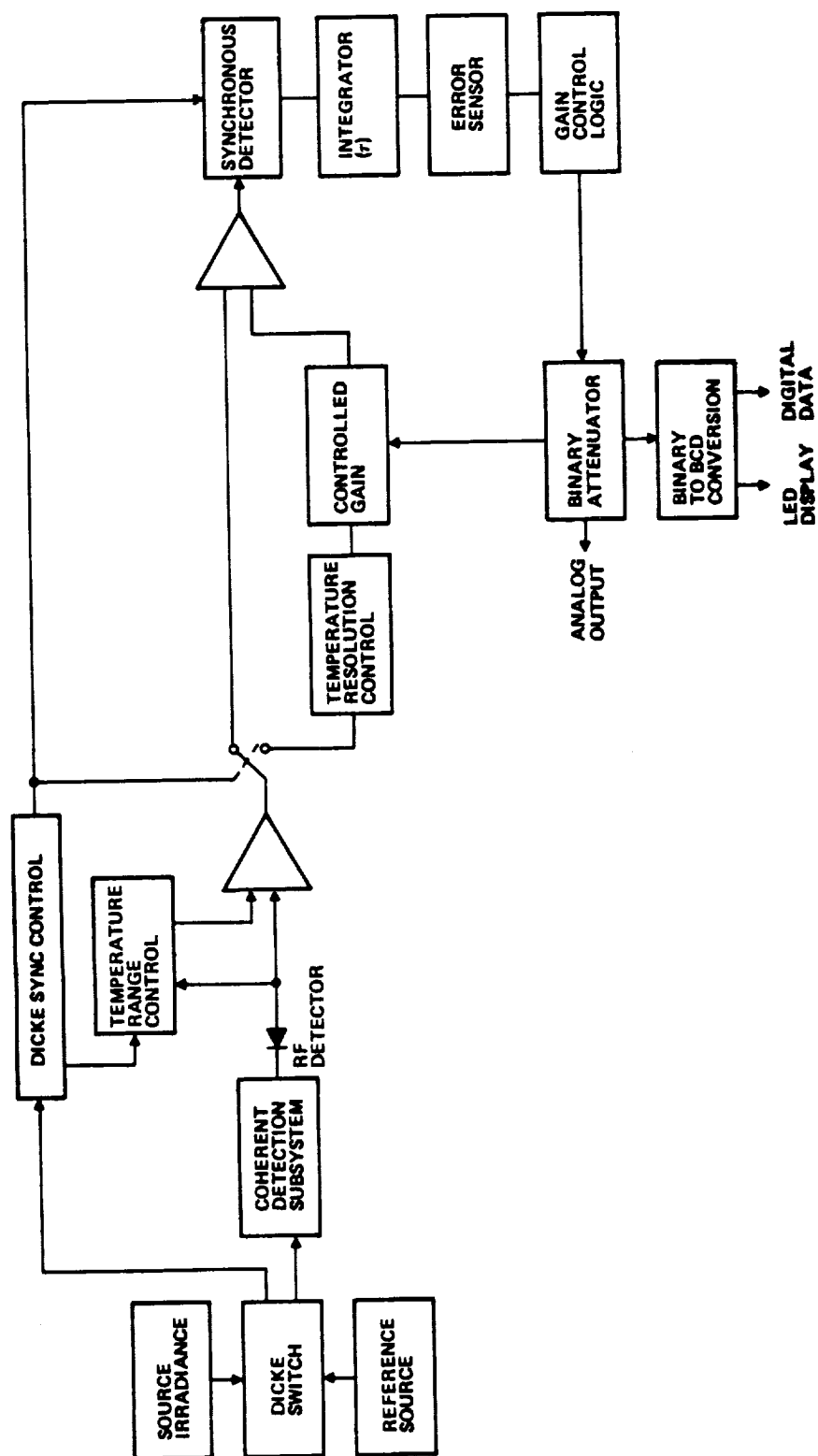
Figure A-5. Simplified Block Diagram of Self-Balancing Gain Modulation Signal Processor
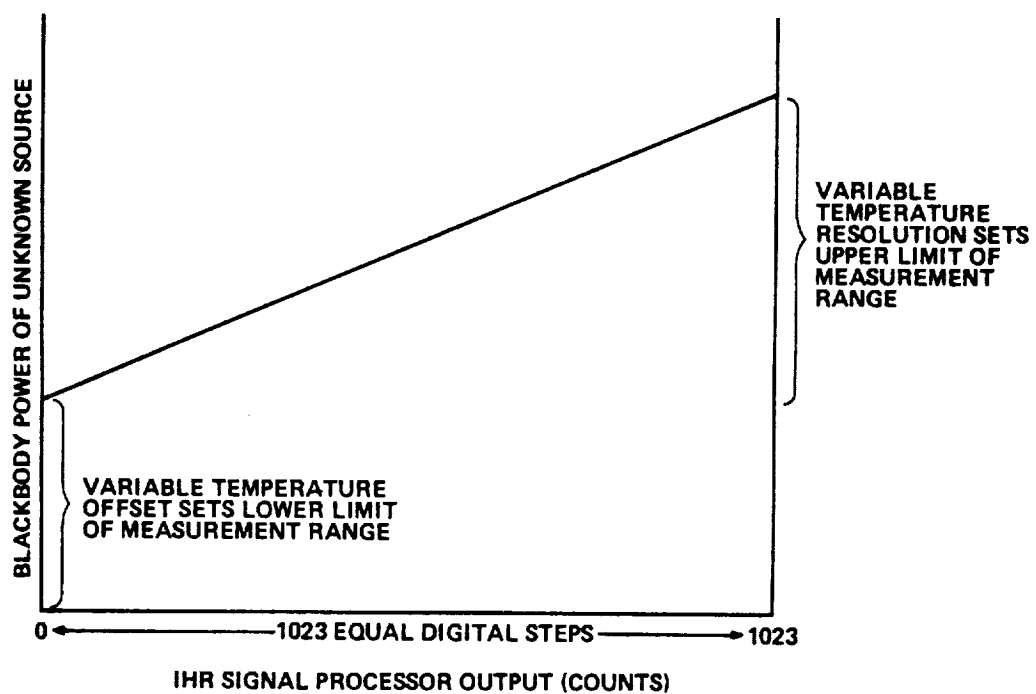
Figure A-6. Radiometer Temperature Range and Resolution for Gain Modulation Mode
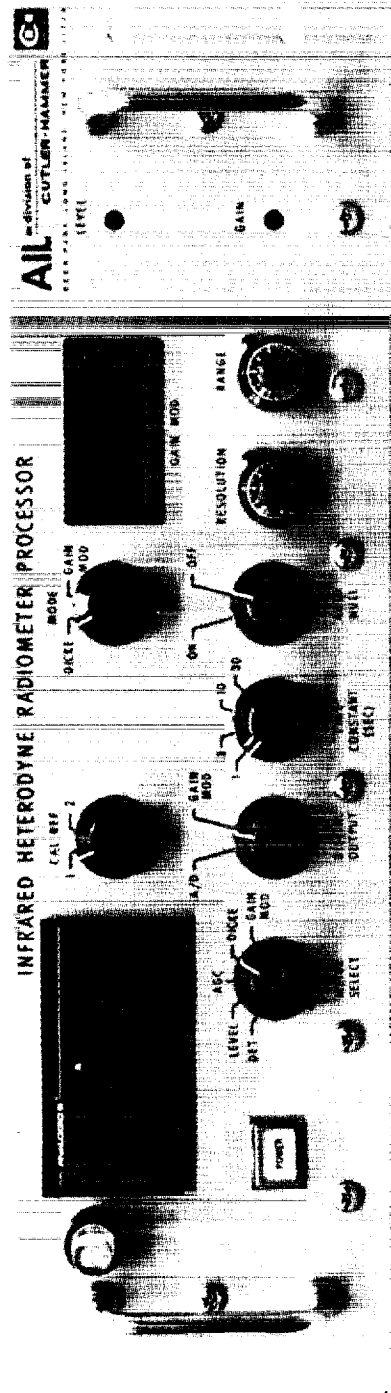
Figure A-7.   Reference Signal Processor Front Panel
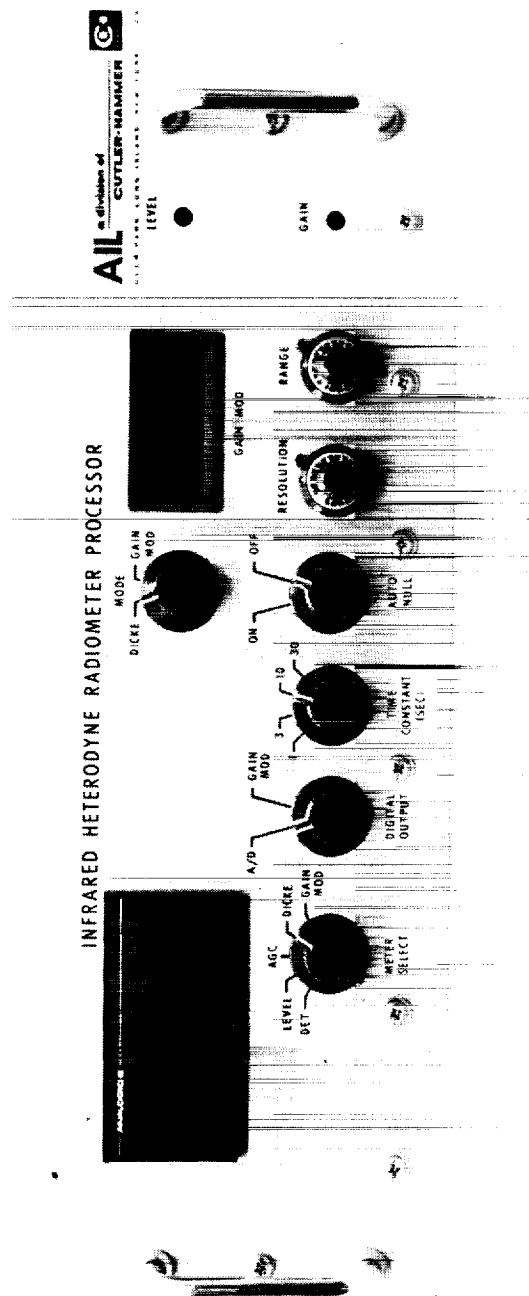
Figure A-8. Pollutant Signal Processor Front Panel

74

Table A-2. Controls Common to Reference and Pollutant Signal Processors

Control	Function
MODE switch	Selects the DICKE or self-balancing GAIN MOD (gain modulation) mode.
METER SELECT switch	Selects the function to be displayed on the front panel digital meter.
A. DET	RF detector output in volts.
B. LEVEL	Monitors the voltage to the comparison amplifier which establishes the AGC voltage (must be $> \approx 5.5$ volts for AGC action).
C. AGC	Monitors voltage to the AGC element in volts.
D. DICKE	Monitors the Dicke output in the Dicke mode or the error voltage when in the gain mod mode.
E. GAIN MOD	Monitors the gain mod analog output in volts.
DIGITAL OUTPUT switch	Selects the panel meter of the gain mod display for output in the serial data stream.
AUTO NULL switch	Disables the self-balancing action of the gain mod mode.
RANGE control	Sets the lowest temperature that may be measured.
RESOLUTION control	Sets the radiometric sensitivity in terms of digits/black body power.
LEVEL control	Adjusts the gain of the processor to establish the correct AGC operating voltage.

Table A-2.   Controls Common to Reference and Pollutant Signal
Processors (cont)

Control	Function
GAIN control	Adjusts overall signal processor gain (does not affect AGC setting).
TIME CONSTANT (SEC) switch	Selects integration time of 1, 3, 10, or 30 seconds.

Table A-3.   Controls Peculiar to Reference Signal Processor

Control	Function
POWER switch	Controls primary power to all channels.
CAL REF switch	Sets the indicating bit in the serial bit stream to 1 or 0 depending on the calibration black body used.

A.4.3   IHR Output Data Display

The IHR output information is displayed on a 3-1/2 digit digital panel meter for the Dicke mode and on a 3-1/2 digit LED display for the self-balancing gain modulation mode.   (Rear panel outputs are also provided.) The LED digital indicator can range in value from 0 to 1023 and is adjustable, with front panel controls, for various temperature ranges and resolutions.   A serial digital output format is also available and is switch selectable between the digital panel meter and the LED display.   Output information is in the form of a 16-bit serial data stream.   The first bit identifies the mode; self-balancing gain modulation (logic 1) or Dicke (logic 0).   The second bit identifies the calibration reference.   The third bit indicates polarity (negative is a logic 1 and positive is a logic 0) in the Dicke mode. The remaining 13 bits contain the data in BCD format (8421).   Each of the radiometer processors updates its output information synchronously ten times per second.   During each of these ten 100-ms intervals, the 16-bit

serial digital bit stream is repeated five times. The first 100-ms interval is invalid, as this is the time interval during which the internal counters are accumulating; this interval is blanked by the data recording equipment. Outputs from the four radiometer processors are sent to the data management unit and tape recorder controller. Here the data is rearranged and control signals for the tape drive are generated. Data buffers are located in the controller and data from the four radiometer channels is recorded once a second. This will allow approximately 8 to 10 hours of data to be recorded on 732 m of tape at 800 bpi NRZI.

A.5 IHR DATA MANAGEMENT SYSTEM

The data management system shown in Figure A-9 consists of three units. These are an Ampex Model TMB 9 track NRZI digital tape transport, an Ampex Model DE840 formatter, and the system interface and controller, AIL Model A610. The Ampex tape drive and format control unit operate in conjunction to provide the correct IBM-compatible tape, recorded in extended binary coded decimal interchange code (EBCDIC). The system interface unit provides for the proper formatting of signal processor data for the Ampex unit as well as supplying the overall control for proper recording of the data. The tape transport holds approximately 732 m (2400 feet) of 1.5-mil thick 0.5-inch wide magnetic tape on a 10.5-inch reel.

A block diagram of the data management system is shown in Figure A-10. Serial data from the four IHR signal processors enter the data management system where it is reformatted into 4-bit words. The data is then stored in a buffer memory. This memory is required in order to match the varying data rates of the tape drive and the signal processors. The memory is loaded and outputted onto the tape once per second. At 800-bpi density, the tape transfer rate required is 10 kilobyte/s. At 200 bpi, the required rate is 2.5 kilobyte/s. Time codes from the aircraft onboard clock are also recorded on the tape for data coordination. The Ampex tape formatter generates the proper tape format. The format control unit ensures that the inter-record gap is approximately 0.6-inch and inserts the cyclic redundancy check character (CRCC), * the longitudinal check character (LRCC), and the vertical check character. During the read operation the formatter uses these check characters to verify the data. The three synchronizing signals from the IHR signal processors are used by the control and timing circuitry to properly reformat the data and load it on the tape in a time synchronous manner with the IHR signal processors.

---

* CRCC is only generated for 800-bpi density.
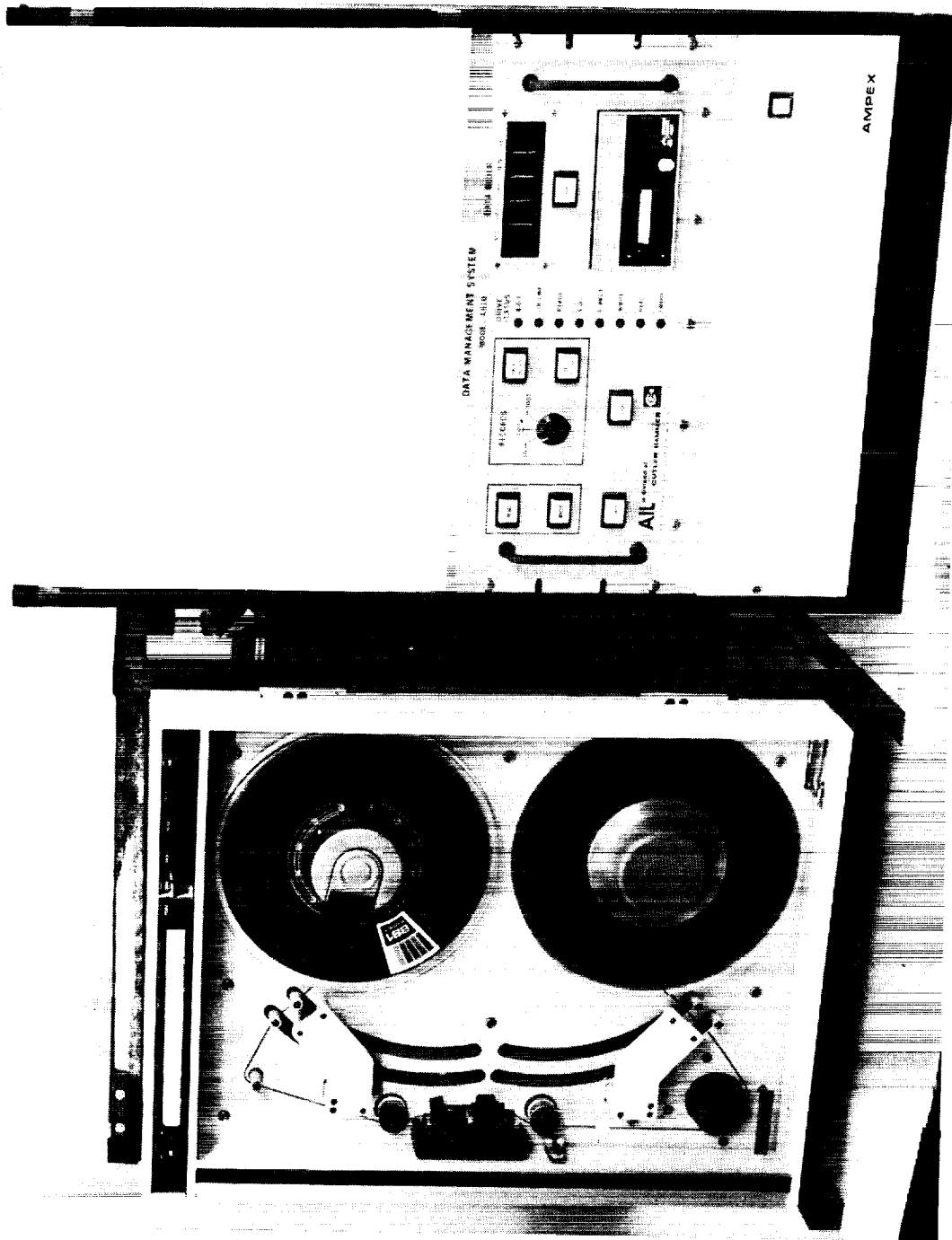
Figure A-9. Data Management System
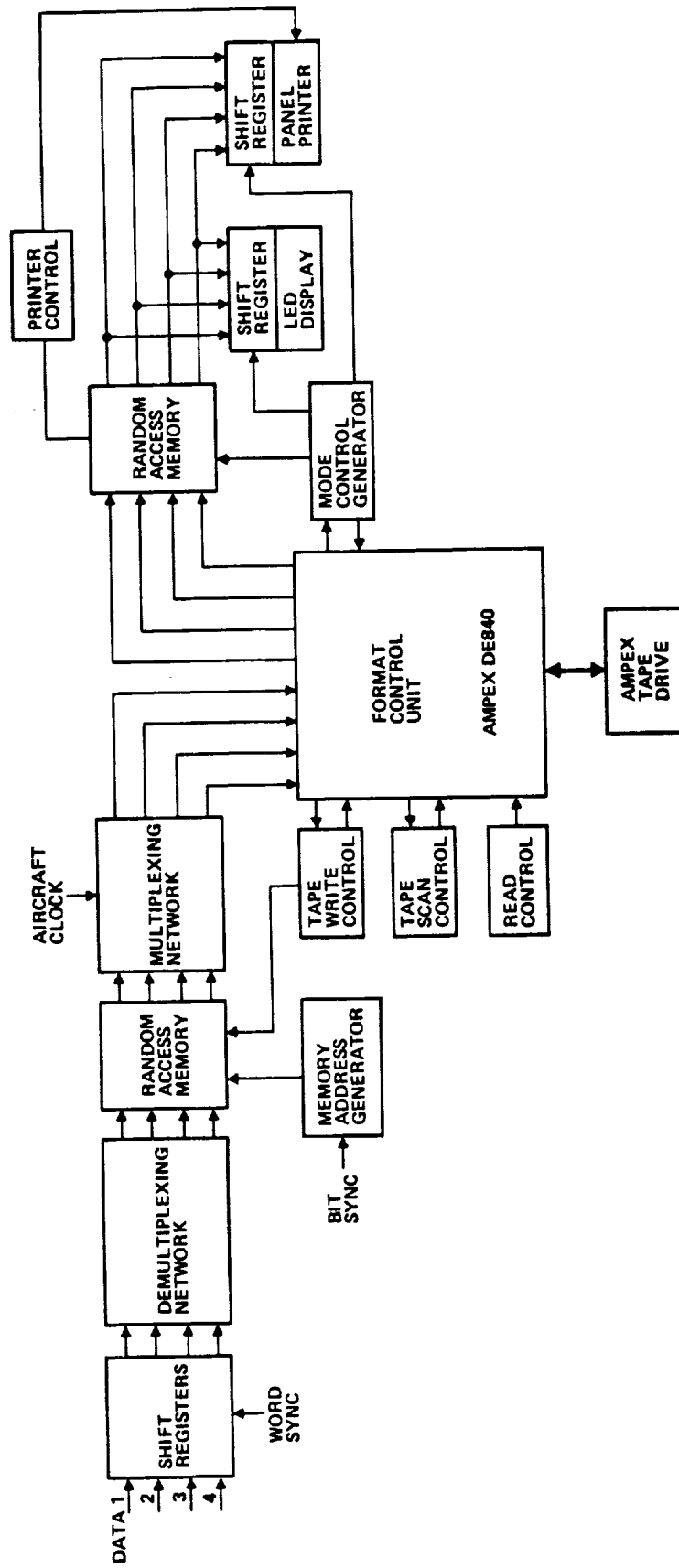
Figure A-10. Simplified Block Diagram of the IHR Data Management Subsystem

79

On output, the data being received from the tape is loaded into a buffer memory, again in a 4-bit word format. Upon completion of the memory load cycle from the tape, the time of the particular data block is automatically displayed on a series of LED's. This occurs by way of a bit serial/word parallel to serial converter. If this represents a data block of interest, a printed copy can be made via the panel thermal printer. Depressing the PRINT switch causes the data to be read from the buffer memory to the panel printer where the data is printed. This allows an operator to scan the tape to a particular area of interest and obtain a limited amount of hard copy data for a more detailed study in the field.

Table A-4 lists the various controls and indicators of the data management system as well as their functions.

Table A-4. Data Management Controls and Indicators

Control or Indicator	Function
B.O.T. indicator	Will be illuminated when the beginning of tape reflective marker is under the transport photosensor.
ONLINE indicator	Will be illuminated when the tape transport is under the control of the data management system.
READY indicator	Will be illuminated when the tape transport is ready to read or write.
E.O.T. indicator	Will be illuminated when the end of the tape reflective marker has passed the transport photosensor.
FPROT indicator	Will be illuminated when the file protect ring has been removed from the tape reel. Data cannot be written onto a protected file.
WRITE indicator	Will illuminate when the tape drive is in the write mode.
READ indicator	Will illuminate when the tape drive is in the read mode.

Table A-4. Data Management Controls and Indicators (cont)

Control or Indicator	Function
ERROR indicator	Indicates an illegal command has been issued to the tape drive. Will also illuminate at the E. O. T.
DATA BLOCK indicator	Indicates the time of a particular data block recorded on the tape.
PRINT switch	Depressing the print switch will cause the panel printer to print a data block.
WRITE switch	Depressing the write switch will cause the tape drive to enter the write mode. It will continue to record the radiometer data until the switch is again depressed.
READ switch	Depressing the read switch will cause the tape drive to read one block of data.
BACK ONE BLOCK* switch	Depressing this switch causes the tape to move one data block in the reverse direction.
SKIP RECORD* switch	Depressing this switch will cause the tape drive to skip forward the selected number of data blocks.
RECORDS switch	Sets the number of blocks skipped forward when SKIP RECORD is pressed.
CLEAR switch	Depressing this switch causes the tape drive command register to clear.
POWER switch	Depressing this switch applies prime power to the data management system. (Note: The tape transport and format control unit will be separately activated.)

* The fast forward and rewind functions on the tape transport can be used to aid in rapidly accessing a particular data record.

81

A.6 PHYSICAL CHARACTERISTICS OF IHR SYSTEM

The IHR system weight is approximately 1100 pounds including support equipment such as water cooler, aircraft mounting fixture, and data recording equipment. The sizes and individual weights are listed in Table A-5.

Table A-5. Size and Weight of IHR System Units

Unit	Qty	Size (inches)	Weight (pounds)
Optical Package	1	24 × 36 × 14	140
Water Cooler	1	14 × 16 × 15	102
Laser Power Supplies	4	7 × 19 × 21	46 × 4 = 184
PZT Power Supplies	2	3.5 × 19 × 13	15 × 2 = 30
Ampex Model TMB Tape Transport	1	24.5 × 19 × 22	110
Ampex Model DE840 Formatter	1	5.25 × 19 × 16	25
AIL Data Management Package	1	8.7 × 19 × 19	25
Photomixer Bias Panel	1	5.125 × 19 × 12	15
Radiometer Signal Processors	4	5.125 × 19 × 21	18 × 4 = 72
Analog Recorder	1	13.5 × 19 × 10	109
1300 K Black Body Controller	1	2.5 × 19 × 10	13
Nadir Black Body Controller	1	7 × 19 × 16	72
TV Monitor	1	5 × 19 × 10	15
Optical Package Mounting Plate	1	36 × 82 × 12	181
TV Camera	1	4 × 6 × 10	6
		Total	1099

Prime 115-Vac power is required at both 400 and 60 Hz with a total maximum consumption of approximately 4 kVA. The power requirement of the individual units as well as their voltages are seen in Table A-6.

Table A-6. IHR Prime Power Requirement

Unit	Voltage (Vac)	Frequency (Hz)	Power (VA)
Optical Package	-	-	-
Laser Power Supplies	115	400	220 × 4 = 880
Water Cooler Neslab RTE-4	115	60	1380 max
PZT Power Supply	115	60	80 × 2 = 160
Photomixer Bias Panel	115	60	140
Ampex Model TMB Tape Transport	115	60	430
Ampex Model DE840 Formatter	115	60	115
AIL Data Management Package	115	60	140
Analog Recorder	115	60	260
1300 K Black Body Controller	115	60	120
Nadir Black Body Controller	115	60	280
TV Camera and Monitor	115	60	30
		Total	3935 max

A.7 REFERENCES

A-1. NASA CV-990 Airborne Laboratory Experimentor Handbook, 1970, NASA Ames Research Center, Moffett Field, California.

A-2. R. H. Dicke, "The Measurement of Thermal Radiation at Microwave Frequencies," Rev. Sci. Instrum., Vol. 17, No. 7, p. 268-275, July 1946.

A-3. T. Orchaug and W. Waltman, Publications of the National Radio Astronomy Observatory, No. 12, p. 179-204, 1962.

APPENDIX B

LATITUDE SURVEY MISSION

In September of 1976, the IHR was shipped to NASA Ames Research Center, Moffett Field, California for installation aboard the CV-990 aircraft "Gallileo II." Gallileo II is NASA's large four engine jet aircraft which serves as a flying laboratory for up to ten simultaneous experiments. This particular field test involving the IHR was designated the Latitude Survey Mission because of its flight itinerary from 80-degrees North latitude to 62-degrees South latitude over the Pacific Ocean. The mission consisted of a series of 14 separate flights from 28 October to 25 November 1976, each lasting an average of 5 to 6 hours. Table B-1 gives the individual flight itineraries and IHR measurement mode.

The IHR arrived 30 September 1976 at NASA Ames and the equipment was unpacked, inspected, and assembled. After a calibration in the laboratory, it was determined that there was no damage to or misalignment of the IHR due to the shipping. A preliminary safety inspection was performed in the laboratory prior to beginning the installation in the CV-990 aircraft. The instrument was found to be in conformance with the NASA safety standards and the instrument was installed on the aircraft.

By Saturday, 16 October, the installation had progressed to a point where the mounted optical package could be checked out. The photomixers were cooled and bias was applied to them. The reference photomixer appeared to operate properly; however, the species photomixer exhibited a higher than normal dark current. This problem was traced to a deterioration of the photomixer I-V characteristic. It was determined that this photomixer would not be suitable for the flight-test program. A replacement was needed. A backup PV:HgCdTe photomixer was obtained from MIT Lincoln Laboratories. This photomixer was mounted in a liquid nitrogen dewar and shipped to NASA Ames along with a spare photomixer available at AIL. The photomixer was integrated into the IHR and the installation continued.

During the aircraft installation period, two germanium windows were checked in an atmospheric pressure chamber for their airworthiness, and were accepted. At the conclusion of the assembly aboard the CV-990, the IHR and its installation were reviewed by the aircraft safety committee and again found acceptable. The windows were then installed in the aircraft and the IHR was then aligned to the solar TV tracking monitor. This was accomplished with the aircraft on the runway utilizing the sun as the external

Table B-1. Flight Itinerary - "Latitude Survey Mission"

Flight No.	Origin	Destination	Measurement Mode
1	Moffett, California	Moffett, California	NR/SA
2	Moffett, California	Fairbanks, Alaska	SA
3	Fairbanks, Alaska	Fairbanks, Alaska	NR/SA
4	Fairbanks, Alaska	Honolulu, Hawaii	SA
5	Honolulu, Hawaii	Honolulu, Hawaii	SA
6	Honolulu, Hawaii	Honolulu, Hawaii	NR
7	Honolulu, Hawaii	American Samoa	NR
8	American Samoa	Melbourne, Australia	NR
9	Melbourne, Australia	Melbourne, Australia	SA
10	Melbourne, Australia	Melbourne, Australia	SA
11	Melbourne, Australia	Christchurch, New Zealand	NR
12	Christchurch, New Zealand	Christchurch, New Zealand	SA
13	Christchurch, New Zealand	American Samoa	SA
14	American Samoa	Honolulu, Hawaii	SA
15	Honolulu, Hawaii	Moffett, California	NR

black body source at infinity. Figure B-1 shows the installation of the optical package and tracker aboard the aircraft while Figures A-4 (Appendix A) and B-2 show the processing and control electronics and the data recording electronics, respectively.

Flight
No.

1 Experimenters Test Flight--On 26 October, an experimenters test flight was carried out to allow checkout of the instruments prior to the flight mission. During this flight, a severe icing problem on the windows was encountered which required rectification before the start of the Latitude Survey Mission. The germanium windows, as well as their aluminum support plates, have a relatively high thermal conductivity and at flight altitude the outside air temperature was on the order of -50°C. This low temperature coupled with the high thermal conductivity caused a thick buildup of condensation on the window surface from the cabin moisture (generated by 38 people on board).

2 Flight to Alaska--Icing problem solved with a directed flow of heated cabin air obtained from the air conditioning ducts. Solar data was obtained on the setting sun toward the end of the flight. The time prior to the measurement was used to calibrate and stabilize the IHR. Difficulties in tuning the lasers were first observed on this flight.

During the flight, the aircraft frequently changed altitude resulting in a change in the aircraft cabin pressure. The control system for aircraft cabin pressure was designed to maintain a fixed pressure differential between the outside air and the cabin air. This resulted in a frequent change in cabin air pressure and therefore the air density. The open cavity laser design contained an air space between the Brewster angle window on one end of the discharge tube and the diffraction grating. As the cabin pressure changed, the air density in the space varied, as did the optical length of the cavity. This variation in optical cavity length resulted in a wavelength change as well as a power output change of the laser LO which the Dicke processor cannot correct. The laser can be retuned for small cavity length changes using a piezoelectric (PZT) cylinder which fine tunes cavity length. This PZT cavity length control was an additional modification to the commercial unit which was added prior to the flight test. For the small pressure and temperature variations

Flight No.	

2
(cont)
experienced at a relatively constant flight altitude the lasers were easily retuned using the PZT. However, it was experienced that large pressure changes corresponding to significant altitude changes could not be simply corrected by a PZT voltage tuning. A manual adjustment of the grating mount was required to re-align the laser cavity and restore the stable power output.

3
Local Polar Flight--Data was obtained on two separate solar tracks over the Arctic Ocean. After the solar runs some initial data was taken in the nadir radiance mode.

4
Flight to Hawaii--The ground-based heating system which was used to keep the plane warm during the night could not cope with the $-18^{\circ}F$ overnight low temperature, allowing the equipment to cold soak. The cold soaking adversely affected the performance of one of the CO_2 laser local oscillators. During this flight, some data was taken in the solar mode. However, the instrument performance was compromised.

5
Local Hawaii Flight--Temporary repairs to the CO_2 laser were made prior to this flight. The repairs were found to be inadequate and severely limited the amount of data taken during the flight.

6
Flight to Samoa--This flight was aborted due to engine failure and the aircraft returned to Hawaii for repairs. Four days were needed to obtain and install a replacement engine. The aircraft downtime was used for some minor operational modifications to the IHR as well as allowing a complete rework of the damaged laser local oscillator. Full performance of the IHR was restored prior to flight No. 7.

7, 8
Flights to Samoa and Australia--These flights had no solar tracking runs and the flight time was devoted to the nadir radiance mode. During these flights, some anomalous data was obtained in the species channel outputs. This anomaly was traced to a local oscillator power reflection. The reference channel functioned properly and appeared to be tracking the broadband (8 to 12 μm) infrared radiometer on the aircraft.

9, 10
Local Australian Flights--These flights were coordinated with local scientific observations which included a balloon launch. Solar data was obtained at the beginning of both of these flights

Flight No.	
9,10 (cont)	at sunrise. The IHR did not behave as well as during the prior sunset tracks which were carried out near the end of the flights. It appears that there is a warmup or stabilization period required at altitude. The solar runs on these particular flights started at the beginning of each of the missions upon reaching flight altitude. Data was obtained on both flights. However, operation of the equipment was much more difficult with the lasers requiring extensive retuning.
11	Flight to New Zealand--Further evaluation of the nadir radiance mode was performed.
12	Local New Zealand Flight--South Toward the Pole--Having obtained a significant amount of data to this point, a decision was made to evaluate an alternate photomixer for the species channel with the possibility of obtaining greater temperature resolution in the higher frequency channels. The change was made prior to this flight and improved high frequency performance was obtained. Data was obtained on three separate CO_2 laser transitions; P(20), P(24), and P(26). The P(20) and P(26) transitions were chosen because they were expected to be the best for solar absorption mode. The P(24) line which is used in the reference channel was also measured in order to get a direct comparison between the reference and the species channel for calibration purposes.

It was on this flight that an extraneous signal was first observed that appeared to limit the accuracy of the ozone measurement data. This solar induced signal is caused by the generation of an interfering signal in the IHR when the instrument is operating in the solar absorption mode. The extraneous signal is believed to be caused by out-of-band solar power reaching the photomixer after being chopped by the Dicke-switch. The heterodyne process, with its associated IF filters, limits the heterodyne signal to an optical bandwidth of 500 MHz. The heterodyne process rejects the extraneous broadband energy which is passed by the optics and the 8-μm long-pass filter which is used to protect the photomixer. However, the solar power passes through the Dicke-switch where it is modulated at the Dicke-switch frequency. This broadband power generates shot noise in the photomixer.

The modulation of this shot noise power level at the Dicke-switch frequency provides an interfering signal similar to that described in paragraph A.1.7 of Appendix A, whose level may be sufficient

Flight No.	

12
(cont)
in some photomixers to influence the solar absorption data. The significance of this effect was only observed at aircraft altitudes where higher solar powers were encountered as a result of a diminished atmospheric absorption above the 30,000-foot flight altitudes. The level of the solar induced signal apparently varies from one PV:HgCdTe photomixer to another.

The interfering signal is wideband in nature and will therefore wash out some of the detail available from the narrowband ozone spectroscopy. It is anticipated that this effect can be corrected in future measurements by inclusion of a narrow infrared band-pass filter to limit the interfering solar energy.

13,14
Flights to Samoa and Hawaii--Solar observations were carried out on these flights using the replacement photomixer. Measurements were made on three local oscillator lines; P(20), P(24), and P(26). Due to the operator experience gained during the previous flights, the time needed to change local oscillator pollutant lines was reduced to the order of 1 minute allowing a significant amount of observation time on each solar run. The solar runs were approximately 1 hour in length.

At the conclusion of the mission, the IHR was off-loaded from the aircraft, packed and shipped back to AIL. The instrumentation arrived safely at AIL on 26 November 1976, and was reassembled in the solar tracking laboratory. Detailed test and calibration measurements were carried out to evaluate the flight worthiness of the IHR package. No performance deterioration was noted during these measurements.

The IHR was then modified in preparation for use on the ASSESS II CV-990 airborne mission (Simulated Space Shuttle Experiment). These IHR modifications included: (1) the investigation of sealed-off, grating tunable, waveguide CO_2 laser LO's and (2) redesign of the package to allow the radiometer to be operated from a remote location by an operator (payload specialist) who was not intimately familiar with the equipment.
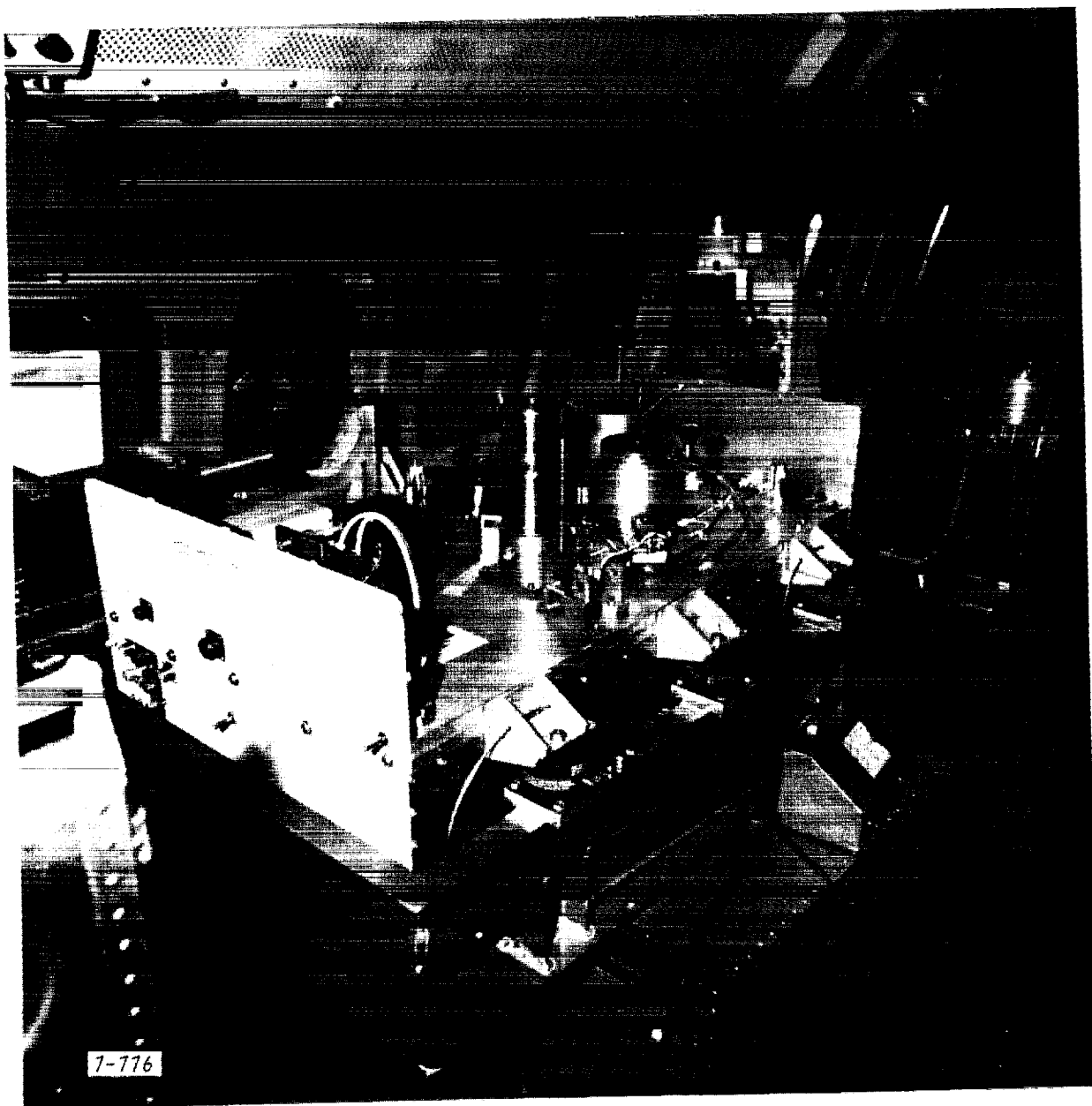
Figure B-1. IHR Optical Package Installation Aboard the NASA CV-990 Test Vehicle

Figure B-2. Data Management Subsystem Installation Aboard the NASA CV-990 Test Vehicle

REFERENCES

1. R. A. Hanel et al, "The Nimbus 4 Infrared Spectroscopic Experiment," J. Geophysics Res., No. 77, p 2629, 1972.

2. A. R. Barringer, "Optical Correlation Spectrometry for Remote Sensing of Air Pollution," J. Opt.Soc.Amer., No. 60, p.729-730, May 1970.

3. M. C. Teich, "Infrared Heterodyne Detection," Proc.IEEE, No. 56, p.37-46, January 1968.

4. B. J. Peyton et al, "High Sensitivity Receiver for Infrared Laser Communication," IEEE J. Quantum Elec., QE-8, p.252-263, February 1972.

5. F. Arams et al, "Infrared 10.6 Micron Heterodyne Detection With Gigahertz IF Capability," IEEE J. Quantum Elec., QE-3, p.484-492, November 1967.

6. J. H. McElroy, "Infrared Heterodyne Solar Radiometry," Appl.Optics, No. 11, p.1619-1622, July 1972.

7. S. R. Kings et al, "High Resolution Atmospheric-Transmission Measurements Using a Laser Heterodyne Radiometer," Appl.Optics, No. 112, p.1106-1107, June 1973.

8. Th. deGraauw and Van de Staadt, "Infrared Heterodyne Detection of the Moon, Planets, and Stars at 10 μm," Nature Phy. Sc., No. 246, p.73-75, December 1973.

9. D. W. Peterson et al, "Infrared Heterodyne Spectroscopy of CO_2 on Mars," Nature, No. 250, p.128-130, July 1974.

10. M. A. Johnson et al, "10 μm Heterodyne Stellar Interferometer," Phys. Rev. Letters, No. 33, p 1617-1620, December 1974.

11. A. J. DiNardo et al, "An Infrared Heterodyne Radiometer for High Resolution Measurements of Solar Radiation," IEEE J. Quantum Elec., QE-9, p.662, June 1973.

12. M. Mumma et al, "Infrared Heterodyne Spectroscopy of Astronomical and Laboratory Sources at 8.5 μm," Nature, No. 253, p.514-516, February 1975.

13. E. D. Hinkley and R. H. Kingston, "Remote Heterodyne Detection of Gaseous Pollutants With Tunable Lasers," AIAA Paper 71-1079, Palo Alto, California, 1971.

14. R. K. Seals, Jr., "Analysis of Tunable Laser Heterodyne Radiometry: Remote Sensing of Atmospheric Gases," AIAA J., No. 12, p.1118-1122, August 1974.

15. R. K. Seals, Jr. and C. B. Bair, "Analysis of Laser Differential Absorption Remote Sensing Using Diffuse Reflection From Earth," Second Joint Conf on Sensing of Environmental Pollutants, ISA JSP 6675, p.131-137, December 1973.

16. R. T. Menzies and M. T. Chahine, "Remote Atmospheric Sensing With an Airborne Laser Absorption Spectrometer," Appl.Optics, No. 13, p.2840-2849, December 1974.

17. B. J. Peyton, "Atmospheric Monitoring Using Infrared Heterodyne Radiometry," Proc of the International Telemetering Conf, Vol.X, p.403-411, October 1974.

18. D. R. Hitchcock and A. E. Wechsler, "Biological Cycling of Atmospheric Trace Gases," NASA CR-126663, 1972.

19. J. C. McConnel, "Atmospheric Ammonia," J. of Geophy Res, No. 78, p.7812-7821, November 1973.

20. J. L. Marx, "Air Pollution: Effects on Plants," Science, No. 187, p.731-733, February 1975.

21. "Air Quality Criteria for Photochemical Oxidants," Chapter 3, U.S. Department of Health, Education, and Welfare, Washington, D.C., 1970.

22. B. J. Peyton, R. A. Lange, M. G. Savage, R. K. Seals, Jr., and F. Allario, "Infrared Heterodyne Spectrometer Measurements of Vertical Profile of Tropospheric Ammonia and Ozone," AIAA Conference, Los Angeles, California, January 1977.

23. R. K. Seals, Jr., "Analysis of Tunable Laser Heterodyne Radiometry: Remote Sensing of Atmospheric Gases," AIAA J., No. 12, p.1118-1122, August 1974.

24. R. A. McClatchey et al, "AFCRL Atmospheric Absorption Line Parameter Compilation," Environmental Research Paper 434, AFCRL-TR-73-0096, January 1973.

25. F. W. Taylor, "Spectral Data for the ν_2 Bands of Ammonia With Application to Radiative Transfer in the Atmosphere of Jupiter," No. 12, p 1181-1217, 1973.

26. F. Allario and R. K. Seals, Jr., "Measurements of NH_3 Absorption Coefficients With a $C^{13}O_2^{16}$ Laser," Appl Optics, No. 14, September 1975.

27. B. J. Peyton et al, "An Infrared Heterodyne Radiometer for High-Resolution Measurements of Solar Radiation and Atmospheric Transmission," IEEE J. Quantum Elec, QE-11, August 1975.

28. R. K. Seals, Jr. and B. J. Peyton, "Remote Sensing of Atmospheric Pollutant Gases Using an Infrared Heterodyne Spectrometer," Proceedings of the International Conference on Environmental Sensing and Assessment, Vol.I, p 10-4, Las Vegas, Nevada, 1975.

29. L. Goldberg, "The Earth as a Planet," G. P. Kuiper, ed., Univ. of Chi. Press, 1954.

30. J. Wolczok et al, "Infrared Heterodyne Radiometer for the Measurement of High Altitude Atmospheric Transmission at HF/DF Chemical Laser Wavelengths," Twenty-Sixth National IRIS, Air Force Academy, Colorado, May 1978.

31. F. I. Shemabukuro et al, "Atmospheric Transmission Measurements at HF and DF Laser Wavelengths," Applied Optics, Vol.15, No. 5, p.1115-1117, May 1976.

32. D. Yustein, W. Chiou, and B. J. Peyton, "Atmospheric Temperature Profiling Using an Infrared Heterodyne Radiometer," Proceedings of the Society of Photo-Optical Instrumentation Engineers, Vol.95, p.105-114, San Diego, California, August 1976.

33. J. M. Hoell, Jr.; F. Allario; and R. A. Lange; "Computer Simulated Vertical Temperature Profiles Obtained by Infrared Heterodyne Techniques," 15th Aerospace Sciences Meeting, Los Angeles, California, 24-26 January, 1977.

1. Report No. NASA CR-3448	2. Government Accession No.	3. Recipient's Catalog No.
4. Title and Subtitle DESIGN, DEVELOPMENT, AND FIELD TESTING OF INFRARED HETERODYNE RADIOMETER (IHR) FOR REMOTE PROFILING OF TROPOSPHERIC AND STRATOSPHERIC SPECIES		5. Report Date July 1981
		6. Performing Organization Code
7. Author(s) R. Lange, M. Savage, and B. Peyton		8. Performing Organization Report No. A610-IV
9. Performing Organization Name and Address EATON CORPORATION AIL DIVISION Walt Whitman Road Melville, New York 11747		10. Work Unit No.
		11. Contract or Grant No. NAS 1-13223
12. Sponsoring Agency Name and Address National Aeronautics and Space Administration Washington, D.C. 20546		13. Type of Report and Period Covered Contractor Report
		14. Sponsoring Agency Code

15. Supplementary Notes

Langley Technical Monitors: Frank Allario and James M. Hoell, Jr.
Final Report

16. Abstract

This report describes the results of a $2\frac{1}{2}$ year analytical, instrument development, feasibility demonstration and flight test program which verified that a new type of radiometer can be employed to remotely monitor the concentration and vertical distribution of selected atmospheric species. The dual-channel Infrared Heterodyne Radiometer (IHR) was developed and flight tested under NASA's Advanced Applications Flight Experiment Office sponsorship.

Ground based solar viewing measurement using the IHR were performed at selected laser transitions for ammonia (NH_3 and ozone O_3). Flight tests were conducted aboard the Gallelio II, NASA Ames CV-990, on the Latitude Survey Mission.

Ozone was the selected atmospheric species for the airborne flight measurements because of the scientific interest in this atmospheric species, the availability of in situ monitors, the coordinated ozone measurements, and the availability of ground truth data. The IHS was operated in: (1) the solar viewing mode to determine ozone distributions in the stratosphere and (2) the nadir viewing mode to determine the ozone distribution in the troposphere. Airborne atmospheric propagation measurements also were carried out at selected CO_2 laser transitions.

17. Key Words (Suggested by Author(s)) Infrared Heterodyne Radiometer (IHR) Solar Absorption (SA) Nadir Radiance (NR) Limb Radiance Solar Occultation	18. Distribution Statement Unclassified - Unlimited Subject Category 45	
19. Security Classif. (of this report) Unclassified	20. Security Classif. (of this page) Unclassified	21. No. of Pages 102	22. Price A06